Energy balance of fusing silver wires surrounded by air

th

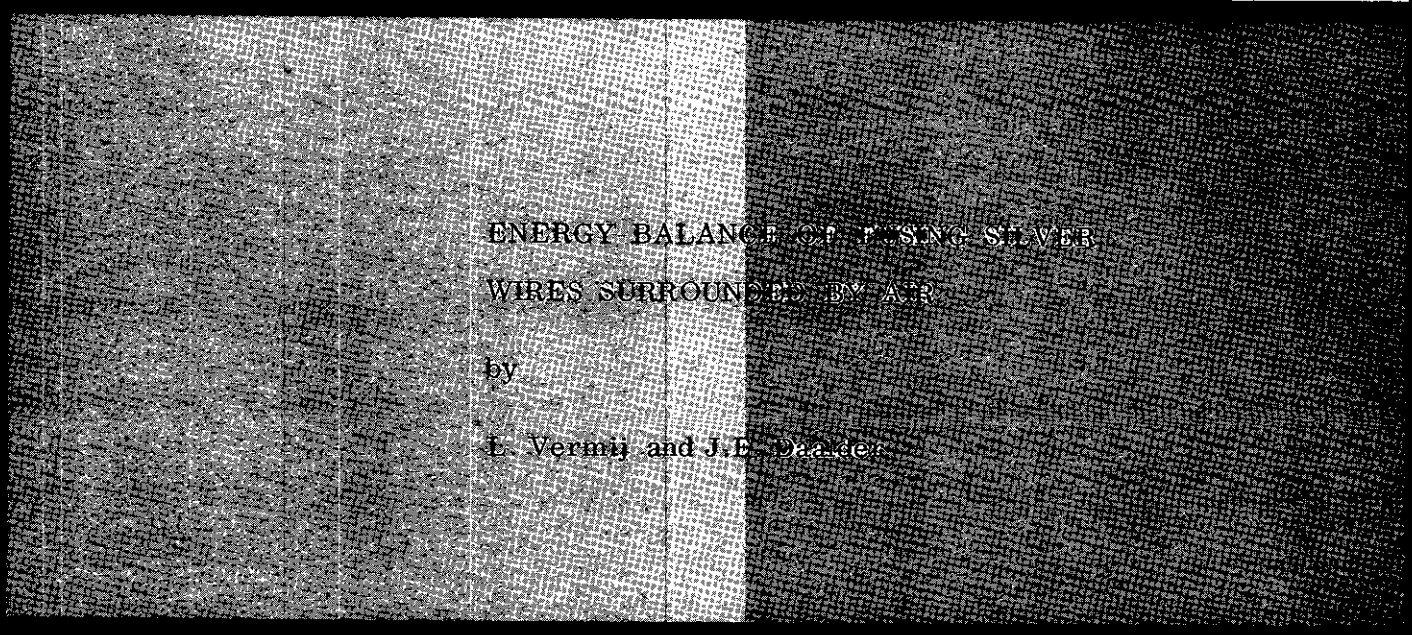

ENERGY BALANCE OF [illegible] SILVER WIRES SURROUNDED BY AIR

by

L. Vermij and J.E. Daalder

ENERGY BALANCE OF FUSING SILVER WIRES SURROUNDED BY AIR

by

L. Vermij and J.E. Daalder

TH-Report 68-E-05

November 1968.

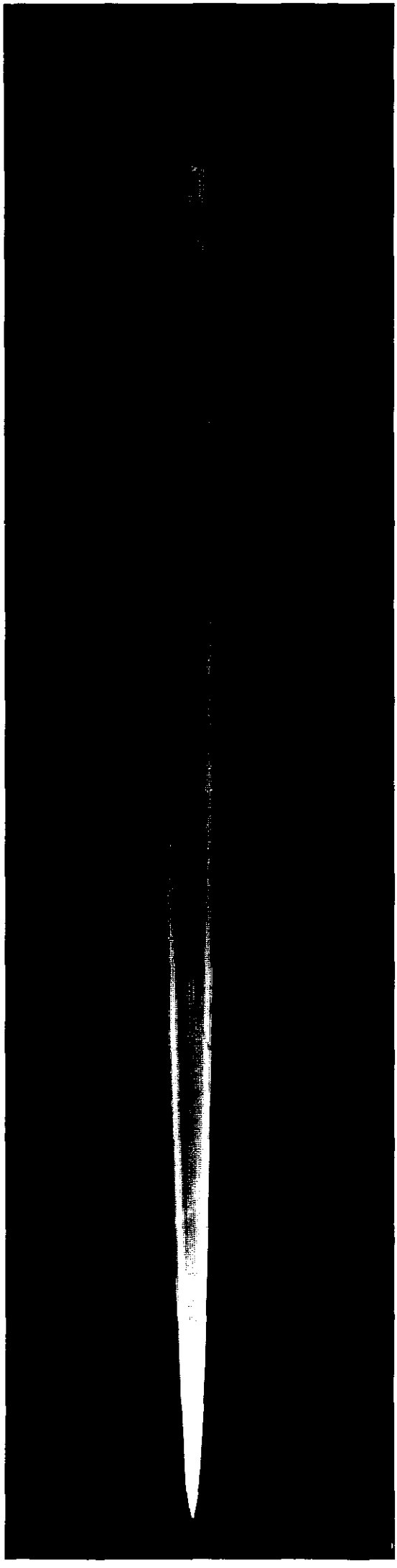

FIG. 3.3.4

ENERGY BALANCE OF FUSING SILVER WIRES SURROUNDED BY AIR

By L. Vermij and J.E. Daalder.*)
(University of Technology of Eindhoven,
Department of Electrical Engineering)

1. Introduction

During the fusing process of a metallic conductor of small cross-section by a fairly strong electric current, the following phenomena can be distinguished:

a. Heating of the wire from ambient to melting temperature,
b. melting of the wire,
c. heating of the wire to boiling temperature,
d. evaporation of the wire,
e. expansion of the metal vapour.

These processes are connected with changes in resistance of the metal conductor. Alteration of the resistance results in variation of voltage drop across the wire. Current variation may also occur, dependent on the magnitude of the variation of the resistance relative to the parameters of the circuit the wire forms part of.

In general, current and voltage can be measured directly. Phenomenological knowledge, dealing with current and voltage changes is sufficiently available.
In order to find an explanation of these phenomena, we have to investigate the governing physical processes.

A clear insight into how the resistance varies until the wire starts to evaporate already exists. This is not the case for the behaviour of the resistance during evaporation and expansion of the wire vapour.

*) A great deal of the experimental work served as a partial fulfilment of the requirements for an M.Sc. degree in Electrical Engineering for J.E. Daalder.

However, it is largely by these latter processes that the performance of a fuse is defined.

The present paper deals with investigations regarding the behaviour of the resistance of the wire from the moment the wire evaporates completely. So we consider the expansion stage of the metal vapour. The work is restricted to cylindrically shaped silver wires, melted and evaporated by a strong electric current, supplied by an LC-circuit with a low ringing frequency (500 Hz).
The wires were kept in air of atmospherical conditions. The work is further restricted to conditions as found in fuses. No consideration is given to a possible application of the results to "exploding wires".

In chapter 2 a discussion of an energy balance equation will be given. The experimental techniques and results will be presented in chapter 3. Chapter 4 deals with the evaluation of these data, in comparison with results reported in chapter 2. Chapter 5 summarises the conclusions of the investigation.

2. The energy balance of an evaporated metal wire

2.1. The energy balance equation

Consider a fusing wire carrying an electric current, which causes the wire to evaporate completely. The condition that the wire has just been evaporated completely is the starting point of our discussion. So we do not consider the evaporation process itself or any previous phenomenon.

We make the following assumptions.

a. The metal vapour is allowed to expand freely (as will be the case in air under atmospheric conditions).

b. Heat transfer to the surroundings of the wire is negligible. This means the wire is only considered during a relatively short time after evaporation.

c. Thermodynamic equilibrium exists in the metal vapour column.

d. The temperature T and consequently also the specific resistance is independent of the radius of the discharge at any instant during expansion. At the circumference of the discharge the temperature changes rapidly from T to the ambient temperature T_o.

With the above assumptions for a free expanding discharge without heat exchange with the surroundings, the energy balance per unit length is given by

$$I^2 R_f = M \frac{d}{dt} (c_v T) + \Delta p \frac{dA}{dt} \qquad (2.1.1)$$

where M : total mass of the wire per meter (kg m^{-1})

c_v : specific heat per unit mass at constant volume (J $^oK^{-1}$ kg^{-1})

A : cross section of the discharge (m^2)

Δp : difference between the pressure in the discharge and the ambient pressure (N m^{-2})

R_f : resistance of the discharge per unit length (Ωm^{-1})

I : current through the discharge (A).

The mass M per unit length of the discharge is assumed to be a constant and equal to the mass of the wire in the solid state. So eq. (2.1.1) applies to the case in which the wire is completely evaporated provided the total amount of metal vapour takes part in the conduction of electricity.

We assume c_v to be a constant in the gaseous state, independent of temperature: $c_v = 3/2\,kN$ (k is Boltzmann's constant, N is the number of particles per unit mass). This is actually not so as N depends on the entropy of the vapour. However, for a qualitative treatment this assumption seems to be acceptable.
In order to discuss the energy balance equation (2.1.1) we introduce the dependency of the specific resistance of the metal vapour on temperature from lit. [1]. This dependency is shown in fig. 2.1a, and a reasonable approximation is obtained by a number of straight lines as shown in fig. 2.1b.
Each of these lines is given by

$$\ln \frac{\rho}{\rho_o} = -\beta T \qquad (2.1.2)$$

where ρ_o is an imaginary value of the specific resistance which would appear at $T = 0^oK$. Further, β is the angle of each line with the T-axis. In case the metal vapour is fully ionised, ρ_o and β are small; if it is only weakly ionised ρ_o and β are larger.
With the help of

$$\rho = R_f A \qquad (2.1.3)$$

and taking into account that R_f and A both depend on time, we obtain from (2.1.1) using (2.1.2)

$$I^2 R_f = -\frac{C}{\beta}\left(\frac{1}{A}\frac{dA}{dt} + \frac{1}{R_f}\frac{dR_f}{dt}\right) + \Delta p \frac{dA}{dt} \qquad (2.1.4)$$

where $C = c_v M$, the heat capacity per unit length of the discharge.
From this equation follows

$$\frac{1}{R_f}\frac{dR_f}{dt} = \frac{\Delta p}{\alpha_2}\frac{dA}{dt} - \frac{1}{A}\frac{dA}{dt} - \frac{I^2 R_f}{\alpha_2} \qquad (2.1.5)$$

where

$$\alpha_2 = \frac{C}{\beta}$$

By means of high-speed streak photographs it is possible to obtain the diameter and thus the cross-section of the discharge as a function

fig 2.1.a

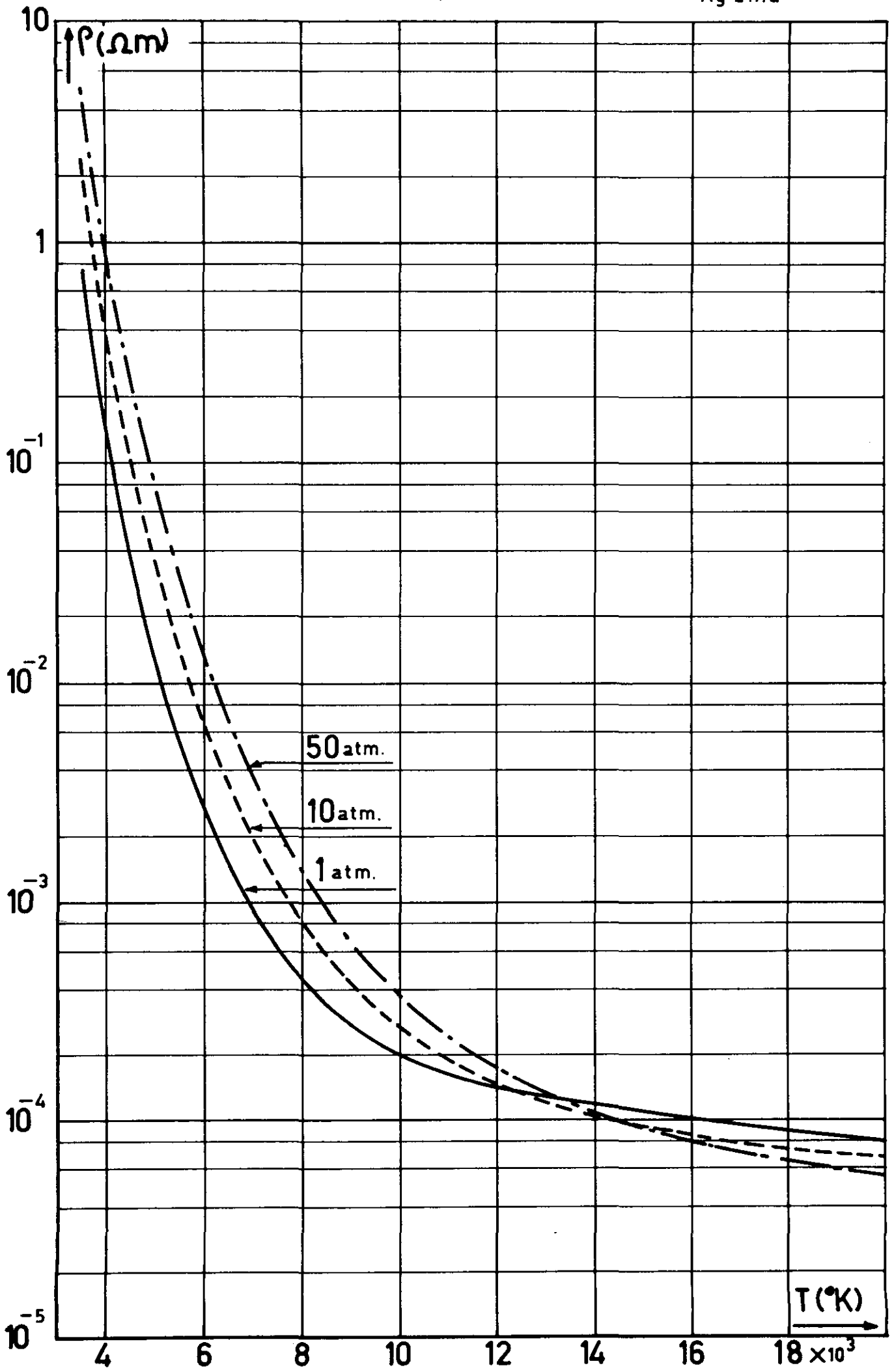
10
ρ(Ωm)
1
10⁻¹
10⁻²
10⁻³
10⁻⁴
10⁻⁵
50atm.
10atm.
1atm.
T(°K)
4
6
8
10
12
14
16
18 x10³

fig 2.1.b

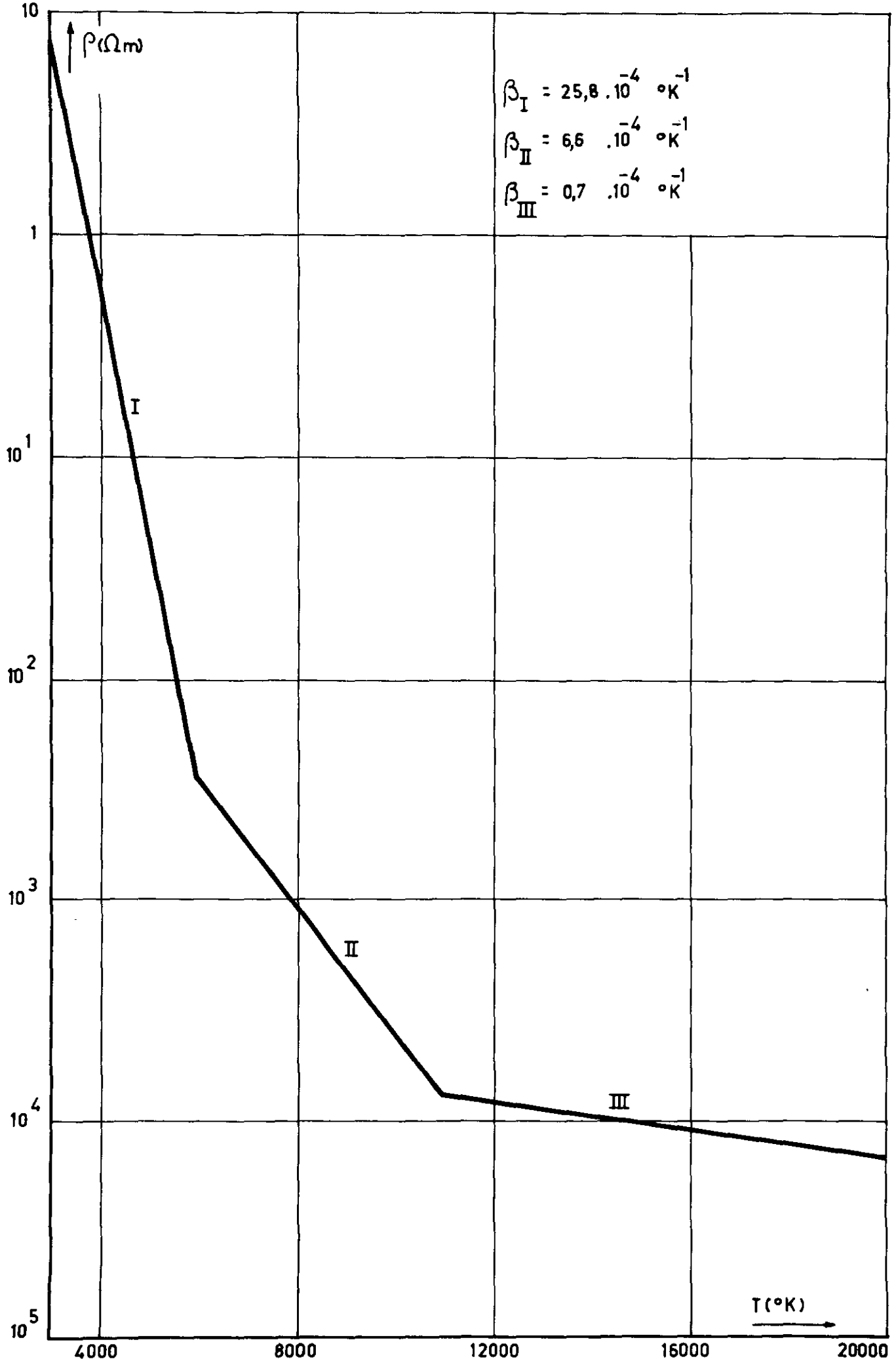
10
ρ(Ωm)
1
10^1
10^2
10^3
10^4
10^5
β_I = 25,8 .10^-4 °K^-1
β_II = 6,6 .10^-4 °K^-1
β_III = 0,7 .10^-4 °K^-1
I
II
III
T(°K)
4000
8000
12000
16000
20000

of time. Oscillograms show the current and resistance of the discharge as a function of time. Moreover, it is possible to determine simultaneously R_f and the cross-section A from experiments, as will be seen in chapter 3.
An expression for Δp is derived in section 2.2. So we should be able to check the energy balance equation (2.1.5) experimentally. This is carried out in chapter 4.

2.2. The pressure and the cross-section of a fully ionised free expanding vapour column

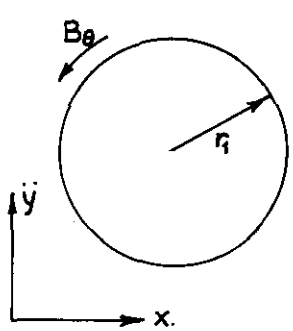

Consider a cylindrical discharge with radius $r_1 = r_1(t)$. The discharge carries a current I_o flowing in the z-direction. The pressure in the discharge ($r < r_1$) may be p(r).
At $r = r_1$ the pressure equals the ambient pressure $p = p_1$. We assume the current densities in the θ and r-direction to be zero, so the current density $J = J_z(r)$.
The current I_o causes a magnetic induction $B = B_\theta(r)$ and $B_r = B_z = 0$.

We start from the Boltzmann transport equations for electrons and ions [2].

$$n_e m_e \left[\frac{\delta \underset{\rightarrow}{v}_e}{\delta t} + \underset{\rightarrow}{v}_e \cdot \nabla \underset{\rightarrow}{v}_e\right] + \nabla p_e + n_e e\left[\underset{\rightarrow}{E} + \underset{\rightarrow}{v}_e \times \underset{\rightarrow}{B}\right] = P_{e \rightarrow i} \qquad (2.2.1)$$

$$n_i m_i \left[\frac{\delta \underset{\rightarrow}{v}_i}{\delta t} + \underset{\rightarrow}{v}_i \cdot \underset{\rightarrow\rightarrow}{\nabla} \underset{\rightarrow}{v}_i\right] + \nabla p_i - Z e n_i\left[\underset{\rightarrow}{E} + \underset{\rightarrow}{v}_i \times \underset{\rightarrow}{B}\right] = P_{i \rightarrow e} \qquad (2.2.2)$$

where n_e ; n_i : electrons, ions per unit volume (m^{-3})
m_e ; m_i : mass of electrons, ions (kg)
$\underset{\rightarrow}{v}_e$; $\underset{\rightarrow}{v}_i$: average velocities of electrons, ions (ms^{-1})
p_e ; p_i : pressure of electrons, ions (Nm^{-2})

e : electric charge of an electron (Coulomb)

Z : charge number

$\underset{\rightarrow}{E}$: electric field strength (Vm^{-1})

$\underset{\rightarrow}{B}$: magnetic induction ($Wb\,m^{-2}$)

$P_{e\rightarrow i}$; $P_{i\rightarrow e}$: total momentum transferred to the ions and the electrons respectively, per unit volume and per unit time

In the equations (2.2.1) and (2.2.2) the gravitational term has been neglected. Furthermore it is assumed that

a. the pressures p_i and p_e are scalar quantities;
b. there exists macroscopic charge neutrality, so $n_i Ze = n_e e$;
c. the total pressure p is the sum of the electron and ion pressures (fully ionised discharge), so $p = p_i + p_e$;
d. the average of the total momentum transfer by collisions with electrons and ions is zero [2], or $P_{i\rightarrow e} + P_{e\rightarrow i} = 0$;
e. there is only one velocity component, viz. the r-component.

So $\nabla \underset{\rightarrow}{v}_i = \frac{\delta v_i}{\delta r}$ and $\nabla \underset{\rightarrow}{v}_e = \frac{\delta v_e}{\delta r}$

From the assumption: $\underset{\rightarrow}{J} = J_z$; $\underset{\rightarrow}{B} = B_\theta$ we obtain $\underset{\rightarrow}{J} \times \underset{\rightarrow}{B} = -J_z B_\theta$ and $\nabla p = \frac{\delta p}{\delta r}$

Adding the equations (2.2.1) and (2.2.2) and substituting (a), the current density

$$\underset{\rightarrow}{J} = e(n_i Z \underset{\rightarrow}{v}_i - n_e \underset{\rightarrow}{v}_e) \qquad (2.2.3)$$

(b) the specific mass

$$\gamma = n_i m_i + n_e m_e \qquad (2.2.4)$$

and (c) the average macroscopic velocity v defined by

$$\gamma v = n_i m_i v_i + n_e m_e v_e \qquad (2.2.5)$$

we obtain

$$\frac{\delta}{\delta t}(\gamma v) - v_i \frac{\delta}{\delta t}(n_i m_i) - v_e \frac{\delta}{\delta t}(n_e m_e) + n_i m_i v_i \frac{\delta v_i}{\delta t} + n_e m_e v_e \frac{\delta v_e}{\delta t} + \frac{\delta p}{\delta r} + J_z B_\theta = 0 \qquad (2.2.6)$$

From the assumption of thermal equilibrium follows

$$v_e = v_i \sqrt{\frac{m_i}{m_e}} \qquad (2.2.7)$$

and

$$v_e \frac{\delta v_e}{\delta r} = \frac{m_i}{m_e} v_i \frac{\delta v_i}{\delta r} \qquad (2.2.8)$$

From eq. (2.2.4) and (2.2.5) we obtain with $n_e = Z n_i$

$$(Z n_e m_i + n_e m_e) v = Z n_e m_i v_i + n_e m_e v_e$$

With $\frac{m_e}{m_i} \ll 1$ this equation becomes

$$Zv = Z v_i + \frac{m_e}{m_i} v_e$$

or, with (2.2.7)

$$v = v_i \left(1 + \frac{1}{Z} \sqrt{\frac{m_e}{m_i}}\right)$$

So with good approximation we may write

$$v \simeq v_i \qquad (2.2.9)$$

Further it follows from (2.2.4) with $\frac{m_e}{m_i} \ll 1$ that

$$\gamma \simeq n_i m_i \qquad (2.2.10)$$

Introducing in eq. (2.2.6) the equations (2.2.8), (2.2.9) and (2.2.10) and the approximation $m_e/m_i \ll 1$, and substituting

$$\frac{\delta}{\delta t}(\gamma v) = \gamma \frac{\delta v}{\delta t} + v \frac{\delta \gamma}{\delta t}$$

we obtain

$$\gamma \frac{\delta v}{\delta t} + (Z+1)\gamma v \frac{\delta v}{\delta r} + \frac{\delta p}{\delta r} + J_z B_\theta = 0 \qquad (2.2.11)$$

In the linearised equation of Spitzer [2] the second term of the equation (2.2.11) does not appear.
Introducing

$$\frac{\delta v}{\delta t} = \frac{\delta v}{\delta r}\frac{\delta r}{\delta t} = v \frac{\delta v}{\delta r} = \tfrac{1}{2} \frac{\delta}{\delta r} (v2)$$

we obtain from (2.2.11)

$$\tfrac{1}{2}(Z+2)\gamma \frac{\delta}{\delta r} (v^2) + \frac{\delta p}{\delta r} + J_z B_\theta = 0 \qquad (2.2.12)$$

With the help of

$$B_\theta(r) = \mu_o \frac{1}{2\pi r} J_z(r)$$

and

$$J_z = \frac{1}{2\pi r} \frac{\delta I_z}{\delta r}$$

equation (2.2.12) transfers to

$$2\pi^2 r^2 (Z+2)\gamma \frac{\delta}{\delta r} (v^2) + 4\pi^2 r^2 \frac{\delta p}{\delta r} = -\tfrac{1}{2}\mu_o \frac{\delta}{\delta r} (I_z^2) \qquad (2.2.13)$$

The quantities γ, v, p and I_z are functions of t and r. So this equation is valid at each instant of time t.
Now we integrate between the boundaries o and r_1 and obtain:

$$2\pi(Z+2)\int_o^{r_1} \pi r^2 \gamma \, d(v^2) + 4\pi^2 \int_o^{r_1} r^2 dp = -\tfrac{1}{2}\mu_o \int_o^{r_1} d(I_z^2) \qquad (2.2.14)$$

I II III

Introducing the total mass $m(r) = \pi r^2 \gamma$ within the radius r, integrating by parts, and realising that a variation in radius r does not result in a change of mass, we obtain for the term I of (2.2.14)

$$2\pi(Z+2)Mv_1^2 \qquad (2.2.14a)$$

where v_1 is the velocity of the periphery of the discharge.
Integrating term II of eq. (2.2.14) by parts we obtain

$$4\pi^2 r_1^2 p_1 - 4\int_o^{r_1} 2\pi r \cdot p \cdot dr$$

where $p = p_1$ for $r = r_1$.
Supposing p is a constant for $o \leq r < r_1$ and introducing

$$A = \int_o^{r_1} 2\pi r\, dr = \pi r_1^2$$

we obtain for the term II of eq. (2.2.14)

$$4\pi A(p_1 - p) \qquad (2.2.14b)$$

In this formula the pressure p can be seen as an average pressure in the discharge.
So we obtain from (2.2.14) with (2.2.14a) and (2.2.14b)

$$2\pi(Z+2)Mv_1^2 + 4\pi A(p_1 - p) = -\tfrac{1}{2}\mu_o I_o^2 \quad *) \qquad (2.2.15)$$

With $A = \pi r_1^2$ and $\mu_o = 4\pi \cdot 10^{-7}$ H/m it follows that

$$2\frac{v_1}{r_1} = \alpha_1 \sqrt{p - p_1 - \frac{I_o^2}{2A} \cdot 10^{-7}}$$

where

$$\alpha_1 = \sqrt{\frac{8\pi}{M(Z+2)}}$$

Introducing $\Delta p = p - p_1$ we obtain also

*) If we assume $v_1 = o$ and $p_1 = o$ then $4\pi pA = \frac{1}{2}\mu_o I_o^2$. Introducing $p = n_e kT_e + n_i kT_i = (n_e + n_i)kT = n_t kT$ and $n_t A = N_t$ we obtain: $4\pi kTN_t = \frac{1}{2}\mu_o I_o^2$. This is the well-known Bennett relation (see [2]). In this equation T is an average temperature and N_t is the total number of particles per unit length.

$$\frac{1}{A}\frac{dA}{dt} = \alpha_1 \sqrt{\Delta p - \frac{I_o^2}{2A} \cdot 10^{-7}} \qquad (2.2.16)$$

Actually this relation is an equation of state of a fully ionised expanding gas column. As a consequence of ionisation and recombination processes the total number of particles per unit volume of this gas column is in principle not a constant.
As mentioned before, A and dA/dt can be determined experimentally. The current I_o is known from oscillographic records. So it follows from (2.2.16) that the difference in pressure Δp can also be found.

3. The experiments

3.1. Introduction

In order to check the energy equation and the equation of state derived in chapter 2, an experimental investigation was set up.
The measurements were carried out on a silver plasma, obtained by the discharge of an LC-circuit in a fusing silver wire. Records of current and voltage gave information over the power input; a rotating mirror streak camera provided a smear to record the diameter of the discharge as a function of time.
These electrical and optical measurements supplied adequate experimental knowledge to determine the time dependent variables in the energy equation.
The experimental techniques, the results obtained and some of the assumptions made, will be discussed.

3.2. The circuit and the electrical measurements

The circuit is shown in fig. 3.2.1. The energy source consists of capacitors with a capacitance of 27.8 μF each having a maximum charging voltage of 15 kV. Current variation was obtained by varying the charging voltage (maximum value 15 kV) and the number of capacitor. The ringing frequency of the circuit was 500 Hz. A trigger spark gap was used as switch.

The electrical recording equipment consists of a current shunt and a voltage divider. The shunt is of the coaxial type, as described by Park [3], and has a resistance of 1.32 mΩ.
The voltage divider is of the type known as mixed type, developed in the High Voltage Laboratory [4].
Both shunt and divider are connected by means of 50 ohm cables with a Tektronix 556 oscilloscope; the shunt has a 50 ohm parallel termination at the oscilloscope, the divider a 50 ohm series termination at the input end of the cable.
Fig. 3.2.2. shows the frequency response of the voltage divider in the complete circuit. An attenuation factor of 580 is taken as an average value for our calculations.

fig 3.2.1

R: shunt 1,32 mΩ
D: voltage divider 1:580
W: wire

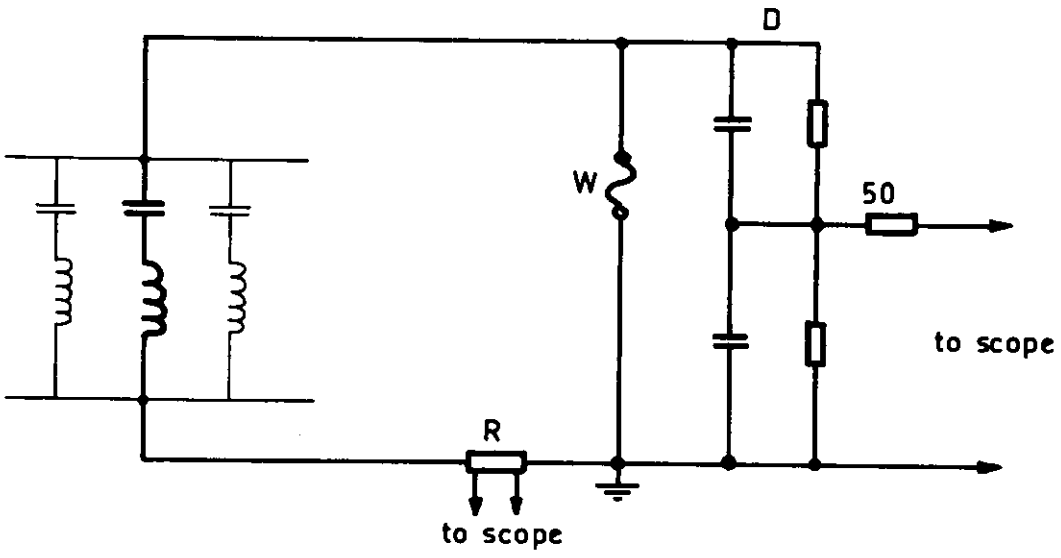

fig 3.3.1

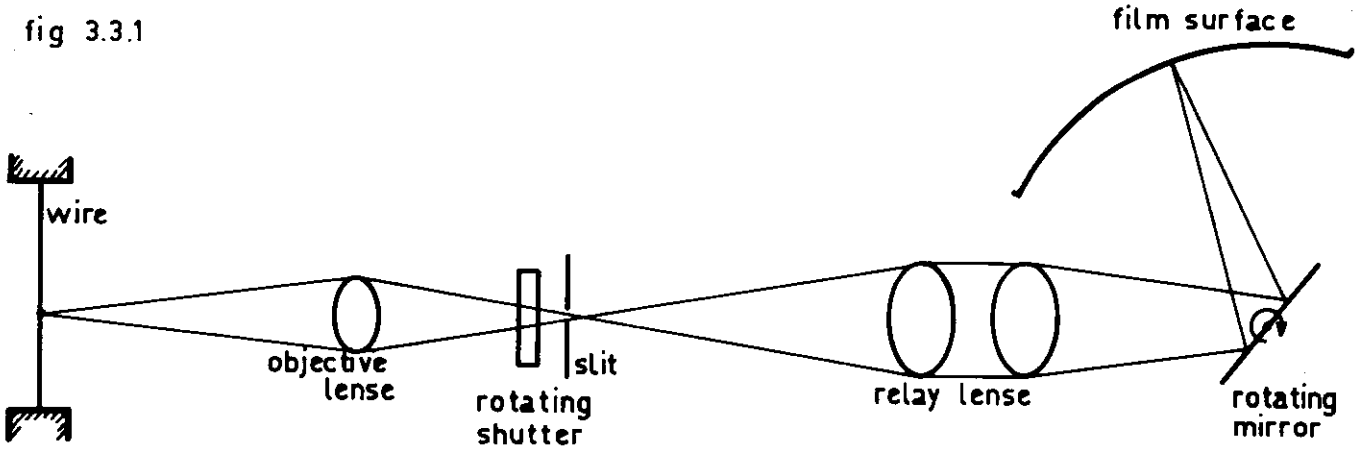

fig 3.2.2

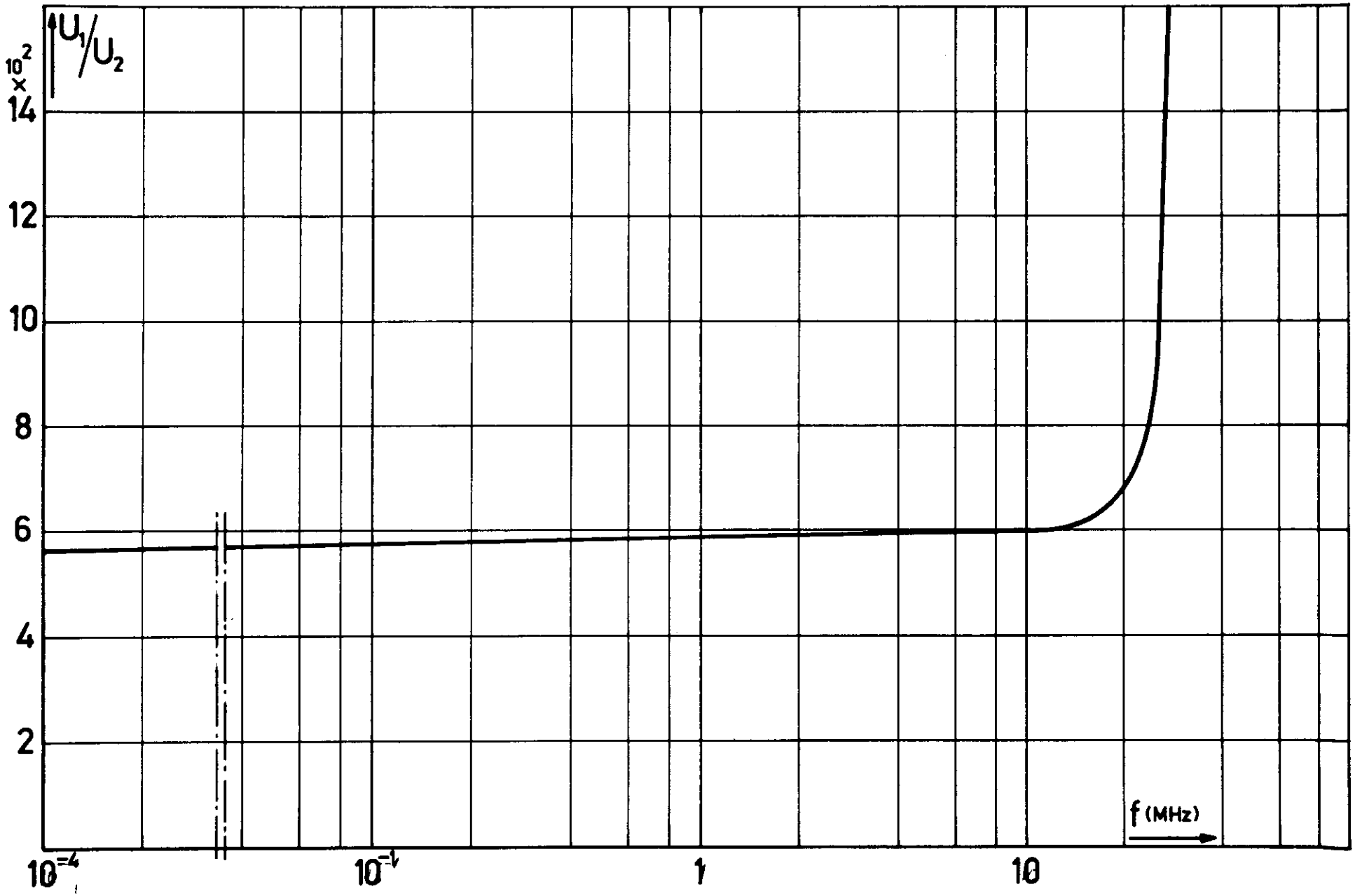

The experimental set-up applied was designed in a coaxial way to prevent disturbances.

Silver wires were used, having a length of 7 cm and various diameters (0.10 - 0.15 - 0.20 mm). The current at which the wires evaporated, ranged from 0.5 kA to 3.0 kA.

Records were obtained on the oscilloscope using a Polaroid camera and a type 47 (3000 ASA) film, also manufactured by Polaroid.

3.3. Optical measurements

In order to obtain data of the radial expansion of the discharge, a Hitachi Uyemura high speed streak camera, model SP 1, was used.
Fig. 3.3.1. shows a general arrangement in the way pictures were made. The holder with its silver wire was placed perpendicularly to the slit of the camera, thus only a small part of the silver column was focussed on the film by the rotating octahedral mirror.
Previous investigations had showed that for this kind of explosions the best results were obtained by using Agfa Record film with a sensibility of 32 DIN. As the process of main interest lasts a few microseconds, only the maximum available writing speed of 4 mm per microsecond was chosen for all the pictures made.

Fig. 3.3.2. shows two representative types of streak pictures. The sole difference between the records is that for fig. 3.3.2a. the aperture was 3.5 and for fig. 3.3.2b. it was 22. All other variables were the same; the silver wire was 0.1 mm in diameter, the camera slit was set to a width of 0.285 mm, the evaporation took place at 1.0 kA.
As we can see, fig. 3.3.2b shows a wedge-shaped image with clearly defined boundaries. Partly, this can also be seen in fig. 3.3.2a, where the wedge-shaped image is surrounded by a luminous shell.
Changing the aperture from 22 to 3.5 means that the light intensity measured on the film plane, has been reduced by a factor 45. Therefore, in fig. 3.3.2a. the luminosity of the shell is much less than that of the core.

Fig. 3.3.2a.

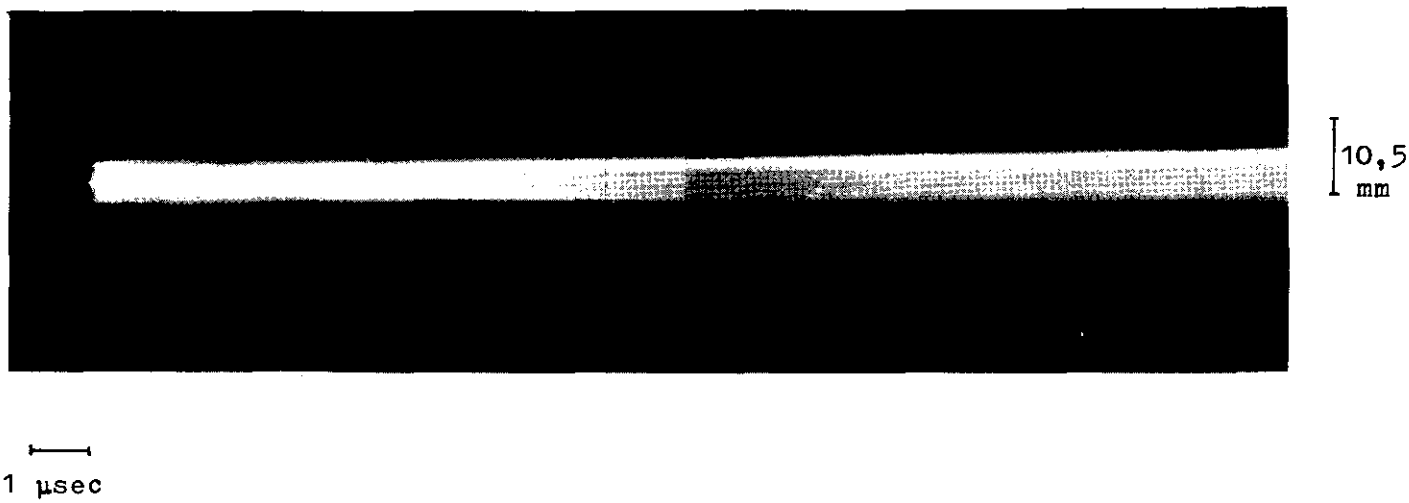

Fig. 3.3.2b.

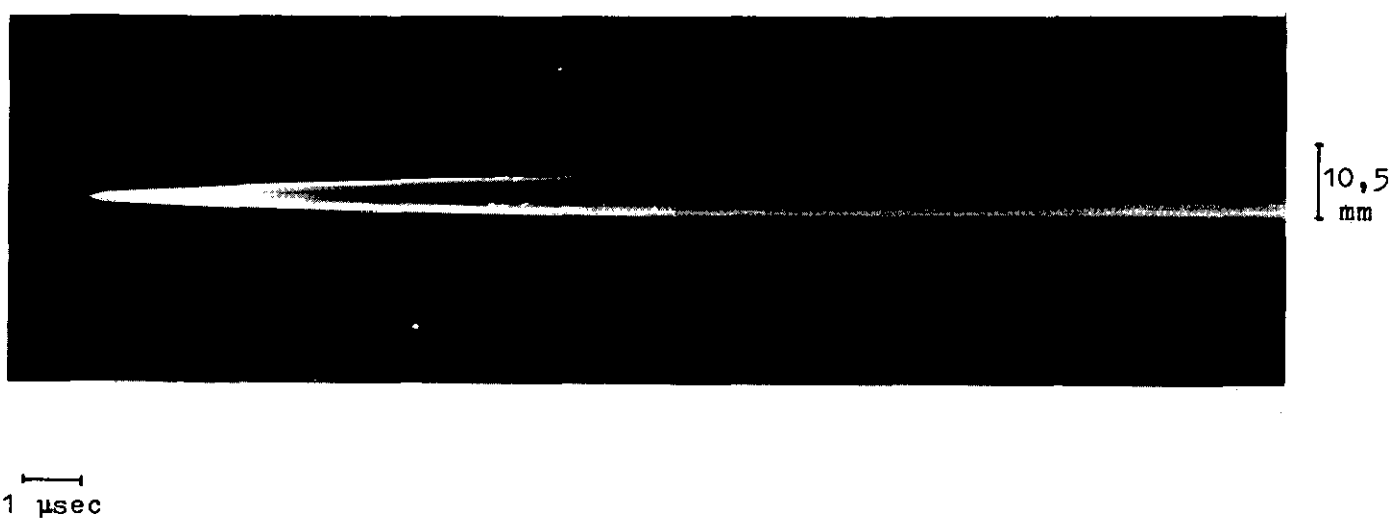

Fig. 3.3.3.

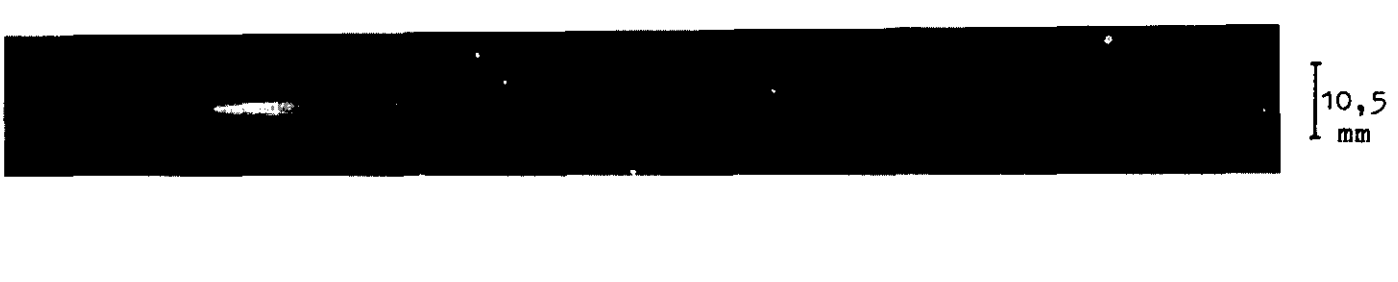

Fig. 3.3.3. shows a streak record, obtained with aperture 3.5 and using a Wratten filter No. 18A between the object and the camera. This filter transmits only light of about 3000 - 4000 Å. Table 1 gives persistent emission lines of neutral and ionised silver and nitrogen with their intensities [5, 18]. We see that two strong lines (resonance lines) of neutral silver are found between the boundaries, given by the filter. As lines of other elements can be neglected, while the spark spectrum of air [5] shows only a few lines of excited oxygen and nitrogen, having a small intensity in this area, it is likely that what is seen of fig. 3.3.3. comes from the emission of neutral silver.
With the instrumental equipment available it proved difficult to show in the same way whether the other persistent lines of neutral silver did occur in the core, i.e. to show that only the core of fig. 3.3.2a. consists of (partly neutral) silver.
As can be seen in table 1, these lines (5210 and 5465Å) lie near lines of single ionised nitrogen. The filters available did not have such small transmitting regions that these lines could be separated. A colour picture (see fig. 3.3.4.) showed that the core has a green colour. The optical density of the shell, being small in comparison with the density of the core, suggests that only very little light coming from the silver vapour will be absorbed by the shell. This means that what can be seen on the colour picture is the emission spectrum of the silver vapour, probably originating from both lines: 5210 and 5465Å, as far as the green column is concerned.

From this we now conclude that the streak record as shown in fig. 3.3.2a can be interpreted as follows. The core represents the expanding silver vapour, partly ionised and surrounded by a shell of air which consists of nitrogen and oxygen atoms and molecules in various states of excitation and, to a very small extent, ionised.
Chase, Lewis and Sleator [6, 7], investigators in the field of exploding wire phenomena, report that besides the presence of metal lines, the emission lines of ionised oxygen and nitrogen do occur, directly after the "time to burst".
Bennet and Shear [8, 9], using an interferometric technique, establish electron densities ahead of the plasma front.
Considering the density of the shell, which is shown by our measurements, it is likely that electrical conductance is maintained by the silver

plasma only. In the nomenclature of Bennett this kind of discharge is called the axial type [12].

Some mechanisms may account for this precursor ionisation. The initial expansion of the wire causes a shock front in the air. The velocities achieved by the metal vapour - the driving gas - make it likely that the temperatures in the shock front attain values at which ionisation is possible [9, 10].
Ultra-violet radiation from the discharge may also account for this. (e.g. 2071Å ($6P^{3/2} - 5^1S_{\frac{1}{2}}$), 2062Å ($6P^{\frac{1}{2}} - 5^1S^{\frac{1}{2}}$) and the whole emission spectrum of single ionised silver which lies between 2000 - 3000Å [5, 18]).
We assume that temperatures in the discharge will not be much higher than 10,000°K, the losses by radiation will then be negligible [11].

Records showing the expansion of this plasma as a function of time, were therefore taken under the same recording circumstances as those under which fig. 3.3.2b was made, giving a clear image of the boundaries to be established.
For calculating purposes, the records were enlarged ten times linearly i.e. a time scale of 40 mm corresponded with 1 microsecond. The enlargement of the wire diameter proved to be 2.1.

Fig. 3.3.2b clearly shows two stages of expansion.
The first part, the sharply defined wedge, lasts 0.2 - 0.4 micro-second depending on current value and wire diameter; the expansion is linear, and high velocities are attained. The second stage is characterised by a much slower expansion. After a transition phase, the diameter versus time is a parabolic function up to about six micro-seconds. For larger times the boundaries deteriorate and the cross-section of the discharge reaches a constant value. This is in accordance with the experiences of various authors (see e.g. [6, 8, 9]).

Fig. 3.3.5 shows the change in diameter of the discharge as a function of time for different values of current and diameter. It was found that for the first micro-second the increase could be very well approximated by linear curves. This makes it easier to establish the cross-section at the transition, which has to be known, as will be shown later.

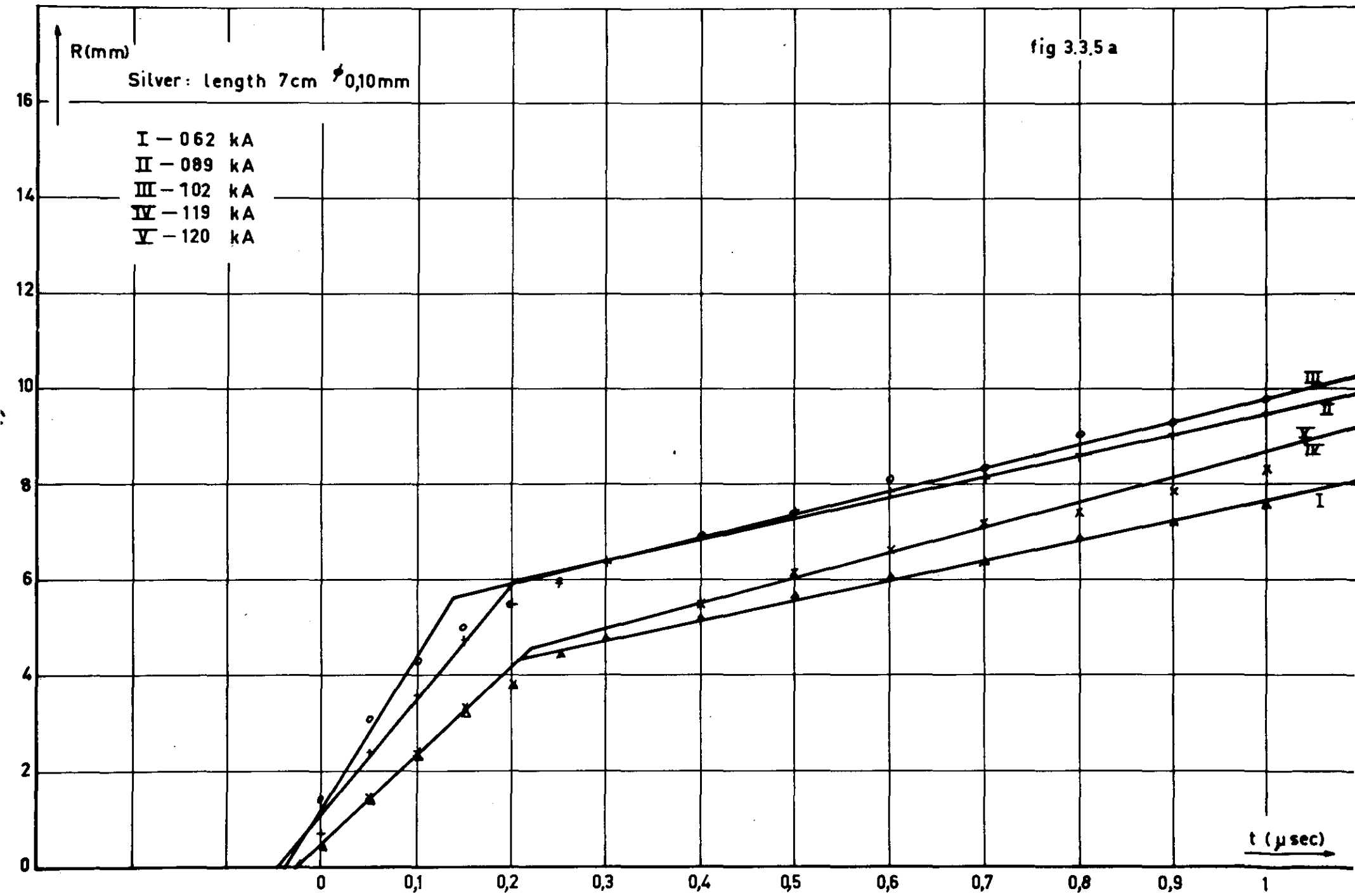
R(mm)
Silver: length 7cm ϕ0,10mm
I — 062 kA
II — 089 kA
III — 102 kA
IV — 119 kA
V — 120 kA
fig 3.3.5 a
16
14
12
10
8
6
4
2
0
0
0,1
0,2
0,3
0,4
0,5
0,6
0,7
0,8
0,9
1
t (μsec)
III
II
V
IV
I

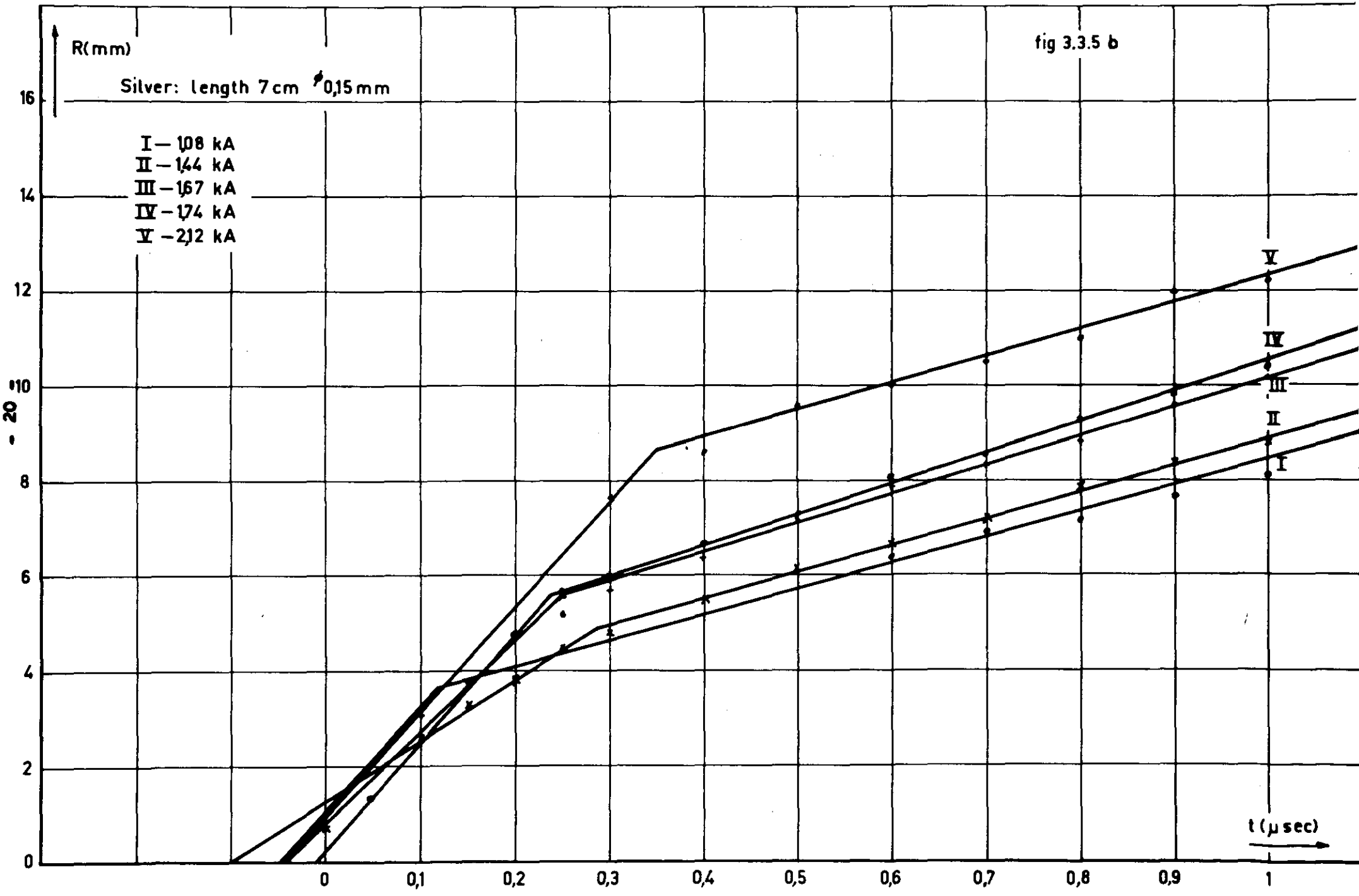
fig 3.3.5 b
R(mm)
Silver: length 7cm ϕ0,15mm
I – 1,08 kA
II – 1,44 kA
III – 1,67 kA
IV – 1,74 kA
V – 2,12 kA
16
14
12
10
8
6
4
2
0
- 20
0
0,1
0,2
0,3
0,4
0,5
0,6
0,7
0,8
0,9
1
t (μsec)
V
IV
III
II
I

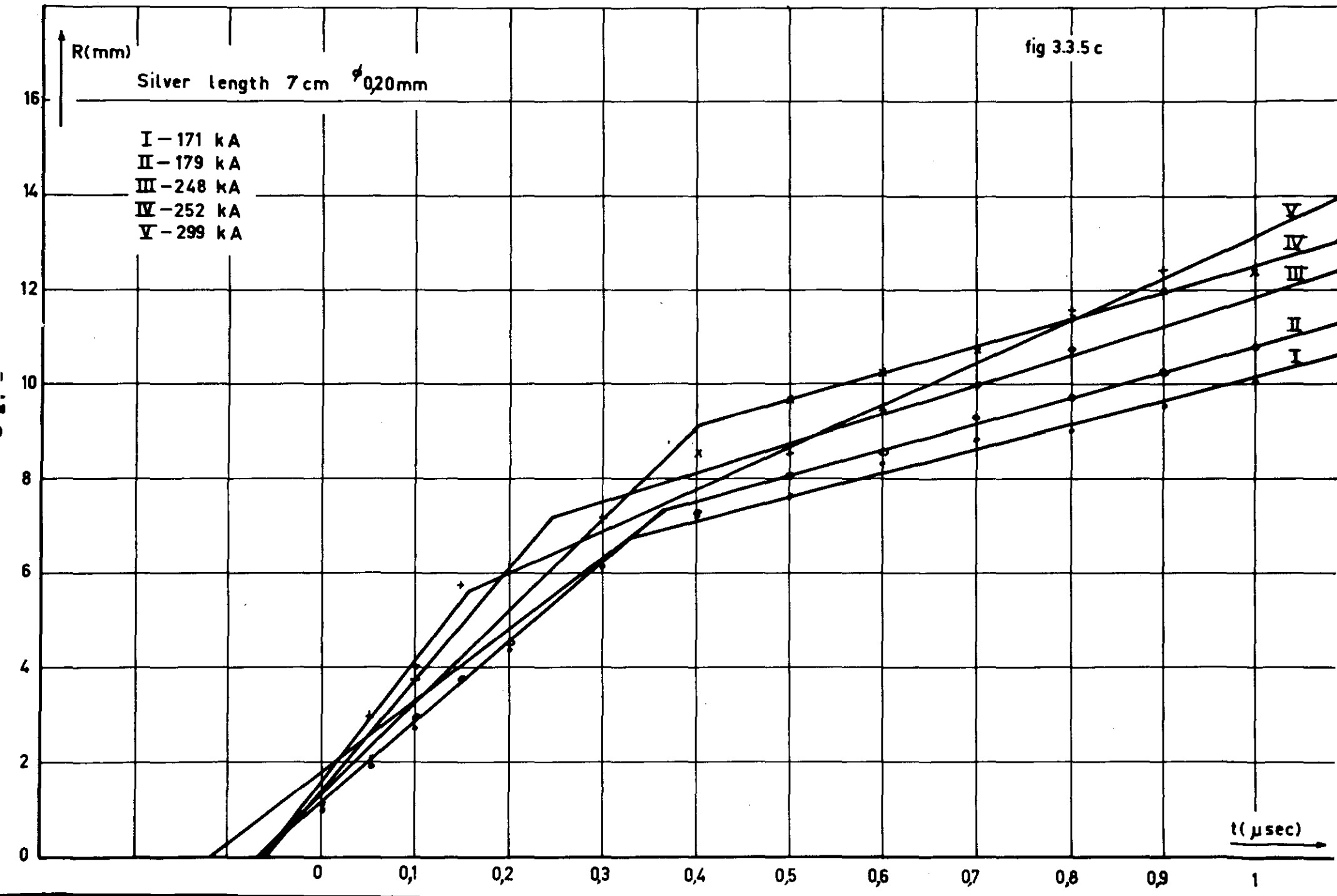
R(mm)
Silver length 7 cm ϕ0,20mm
I – 171 kA
II – 179 kA
III – 248 kA
IV – 252 kA
V – 299 kA
fig 3.3.5 c
t(μsec)
0
2
4
6
8
10
12
14
16
0
0,1
0,2
0,3
0,4
0,5
0,6
0,7
0,8
0,9
1

Table 2 gives an impression of the Mach-numbers for the quicker and the slower parts of the expansion.

3.4. Establishment of a common time base

Fig. 3.4.1 shows an oscillogram of the current passing through a wire and the voltage measured across it. The time base is one micro-second per division. Only the interesting part of the phenomenon has been considered, i.e. the time elapse during which the voltage is changing rapidly. When the current starts to flow, the voltage first remains on a low level until it rapidly rises to a high value and drops again sharply. The largest energy input in the wire occurs also in this region.

An important point is to establish the starting of the discharge. We assume that from that point on we are dealing with a plasma consisting of completely vaporised, and, to a certain extent, ionised, silver. In this region the energy balance previously discussed can be applied.
For that purpose, we established a common time base for both electrical and optical measurements. This was achieved by filming the evaporating wire and the light output of a spark gap at the same time. The spark gap consists of two brass spheres, positioned opposite each other. One of the spheres contains a trigger pin, for this purpose placed at a certain angle, partly outside the area of the sphere.
A pulse generator triggered the gap, enabling the current to flow through the wire.
The position of the pin enabled the initial spark to be filmed by means of an arrangement of mirrors (see fig. 3.4.2). The wire was filmed at the same time. As the pulse used for this spark also started the oscilloscope (triggering by the incoming current signal) synchronisation was thus achieved.
Fig. 3.4.3 shows a record of both the spark gap (i.e. the initial spark and the development of the discharge channel between the spheres) and the expanding wire. During these measurements the slit of the streak camera was 3.5 (The arc between trigger pin and sphere is short and has only little luminosity).
We measured the time elapsed between the initial spark of the gap and the starting of the clearly defined wedge of the expanding wire, as

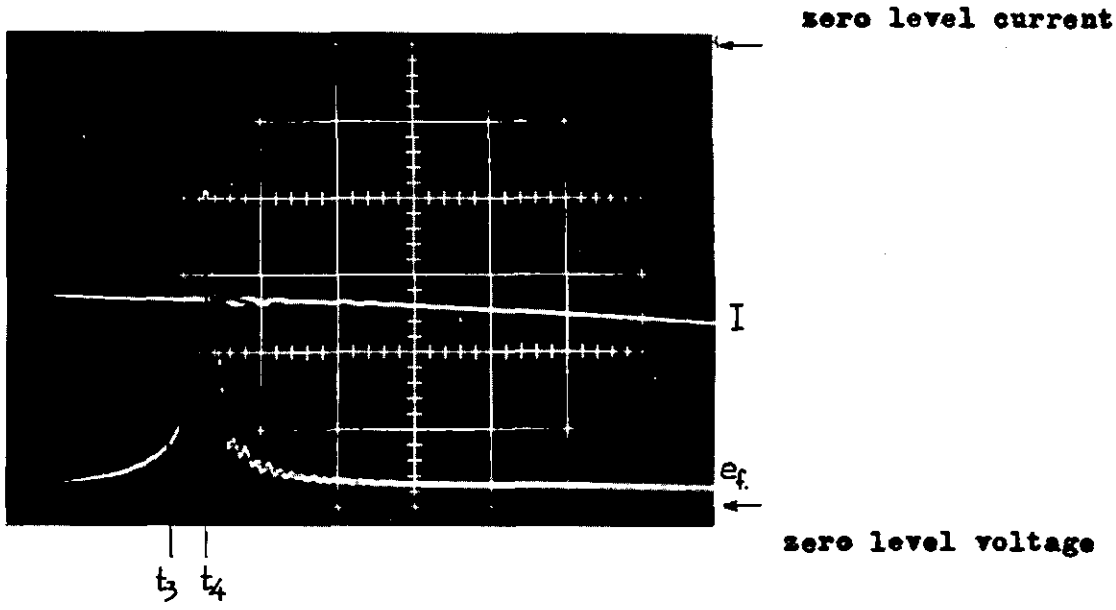

Fig. 3.4.1: Current and voltage traces of a 0.20 mm ø fusing silver wire, 7 cm length.
Time base: 1 µsec/div.
Current: 760 A/div.
Voltage: 5,8 kV/div.

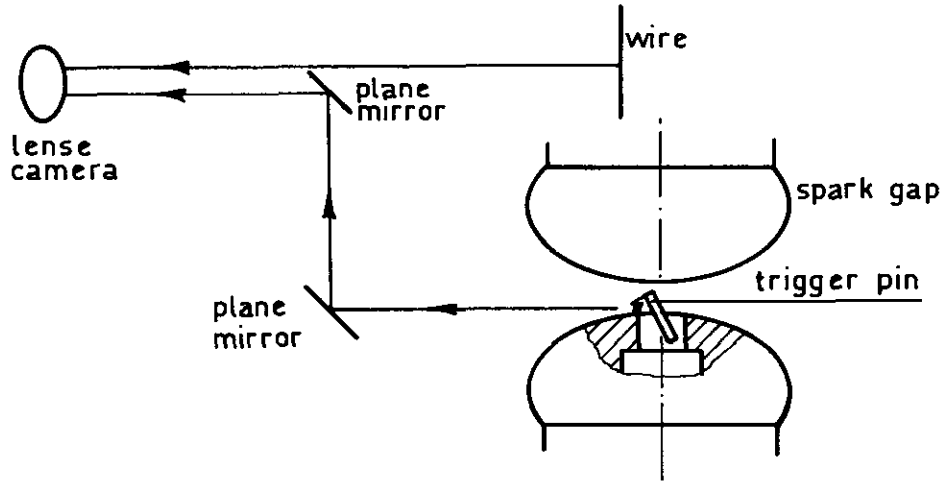

Fig. 3.4.2.

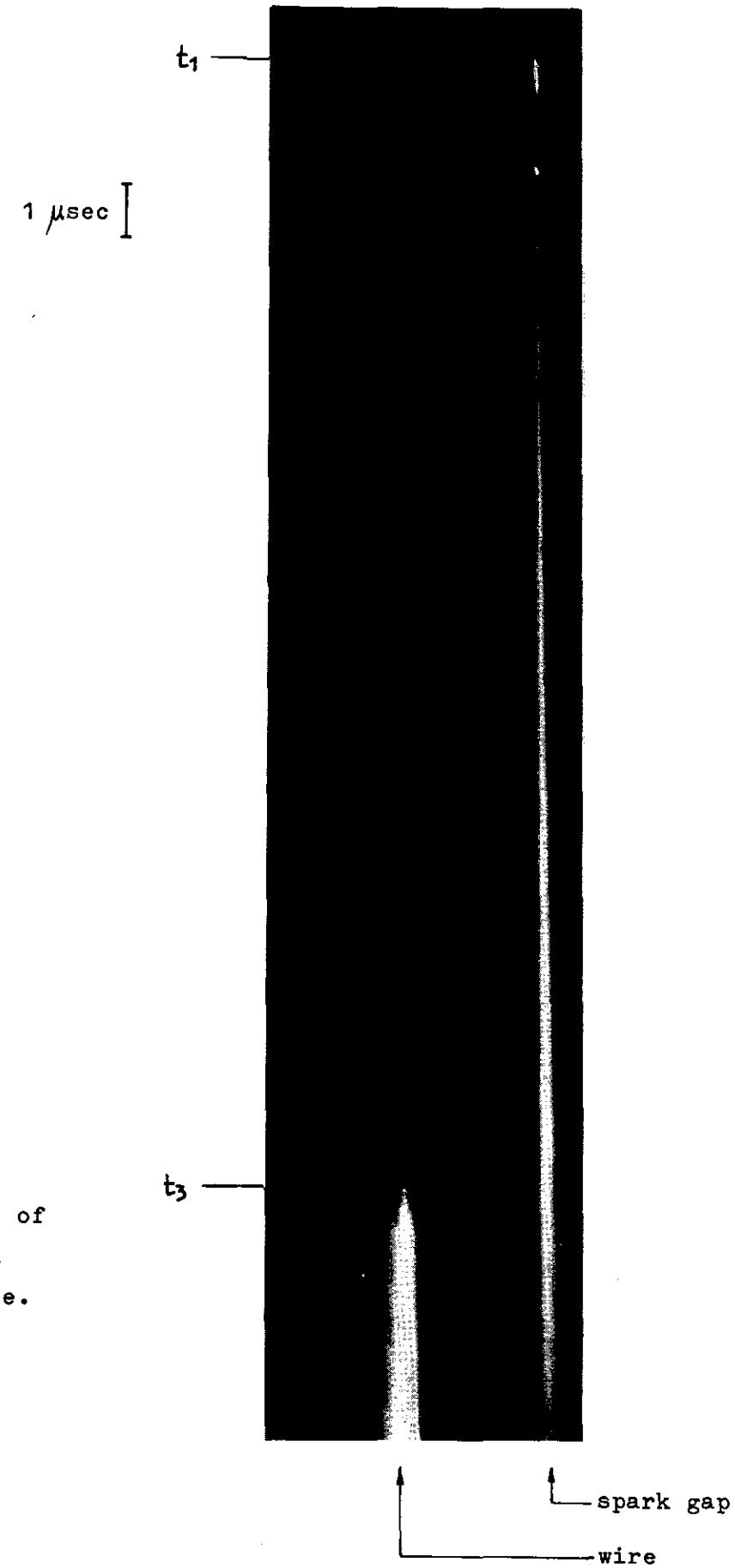

Fig. 3.4.3.

Streak record of spark gap and expanding wire.

shown in the picture. The time the linear expansion takes until the transition to a parabolic time dependency was also computed and added. The accuracy thus achieved was of the order of 100 nanoseconds. At the same time the voltage was recorded on a time base of one microsecond per division, using the delay line of the oscilloscope; the result is shown in fig. 3.4.1. The time interval between the start of current flow and the voltage peak was established. The error in the time calculation is mainly dependent on the accuracy of the delay line. If we assume an accuracy of 1% of full scale, the error made will be 100 nanoseconds or less.
Comparison of the two times, i.e. the time at which the voltage peak occurs and the time of transition of the wire boundary from linear to parabolic expansion, proved to be in reasonable agreement. The measurements were reproducible.
This conclusion is supported by investigations of Bennett et al. [12]. Using a different technique, they obtain the same result, achieving a correlation of electrical and optical records within 30 nanoseconds.
The time the linear expansion lasts, proved to be of the same order as the time in which the voltage reaches maximum value (see fig. 3.4.1, time t_4) from the moment that its slope sharply changes (see fig. 3.4.1, time t_3). High accuracy was not attained for reasons to be discussed in the following chapter.

We now assume that the development of the expansion occurs as follows. Fig. 3.4.4 shows a schematic oscillogram and streak record of a fusing element on a long time base.
Keilhacker proved [13] that at t_2 the wire has completely melted, while t_3 is the moment the evaporation of the wire commences. Our measurements (if correct) show that the moment t_3 coincides on the streak record with the starting of the linear expansion. Keilhacker [13] states that evaporation will start at the circumference of the wire. A situation arises then in which there exists a column of overheated liquid silver, surrounded by a shell of dense silver vapour. The resistance transition from the liquid to the gas phase is very large (factor 100 or more), so the conduction will be maintained mainly by the liquid core. During the process of evaporisation, which occurs very fast (Jäger [14] speaks of a "Stosswelle"), the cross-section of this liquid core diminishes, causing an increasing resistance, sustained by a further rising of the

fig 3.4.4

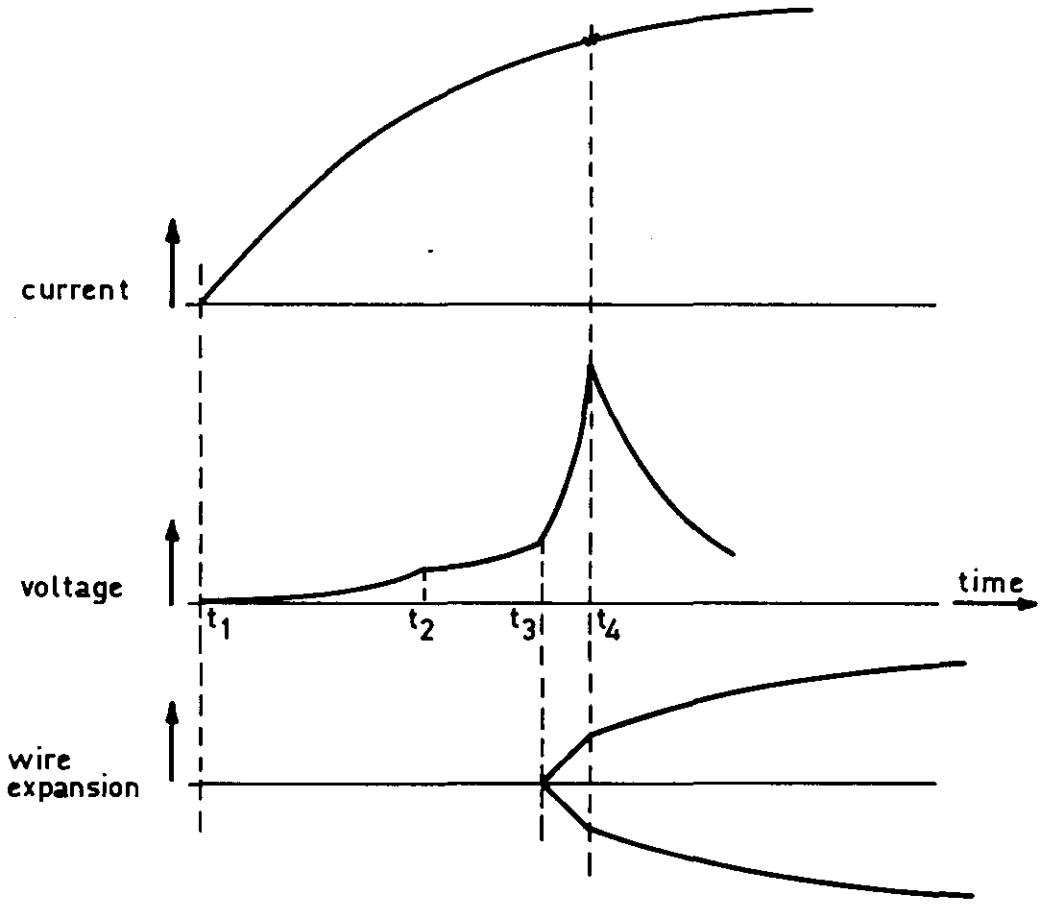

temperature. This process continues until all or nearly all the wire material has been transformed into gas. At that moment the resistance and, accordingly, the voltage, attain their maximum values (at time t_4).

Under the influence of the high voltage developed across the wire a discharge may be formed and the transition of metallic to plasma conduction occurs.
Owing to the expansion of the metal vapour the temperature may drop. Only when the temperature drop is such that the ionisation does not decrease as rapidly as the cross-sectional area of the plasma increases, can the resistance, and consequently the voltage, drop, as is the case here.

We therefore expect that the starting point for the use of the energy balance is that instant where the voltage reaches its highest value, i.e., where the expansion transits from a linear to a parabolic course.

3.5. The uniform expansion of the wire

It should be emphasised that there is an important experimental difference between the electrical and optical records.
The optical measurements show the changes of only a very small part dl of the wire, if l is the length of the wire (In the ideal case, the length of dl should be infinitesimal).
The electrical records, however, represent an integrated effect; the voltage drop across the whole length of the wire is measured.
This indicates that both kind of records can only be compared when the optically measured changes of an element dl are the same for every other element of the wire, or, when the expansion of the wire is independent of its length. Under this condition the energy balance as derived in chapter 1, is applicable.

For that purpose the expansion of the wire as a whole was investigated. It has turned out that for low current values this expansion is not uniform but starts in different places along the wire and at different times (see also [19]).
Fig. 3.5.1, shows a streak record and a matching oscillogram obtained with a silver wire 0.15 mm in diameter. The phenomena indicated above

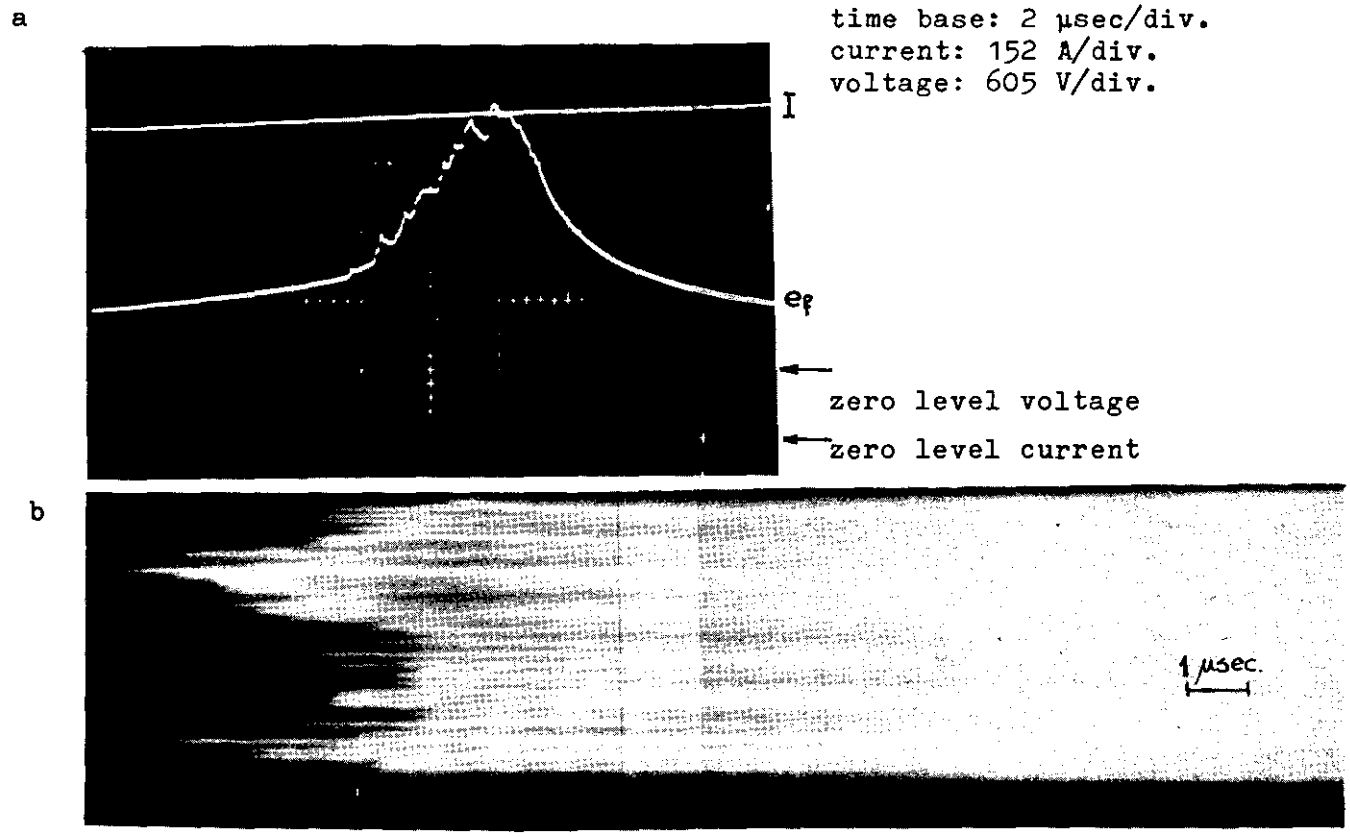

Fig. 3.5.1. Fusing silver wire 0.15 mm ø, 7 cm length.
Current value at the onset of the discharge: 710 A.

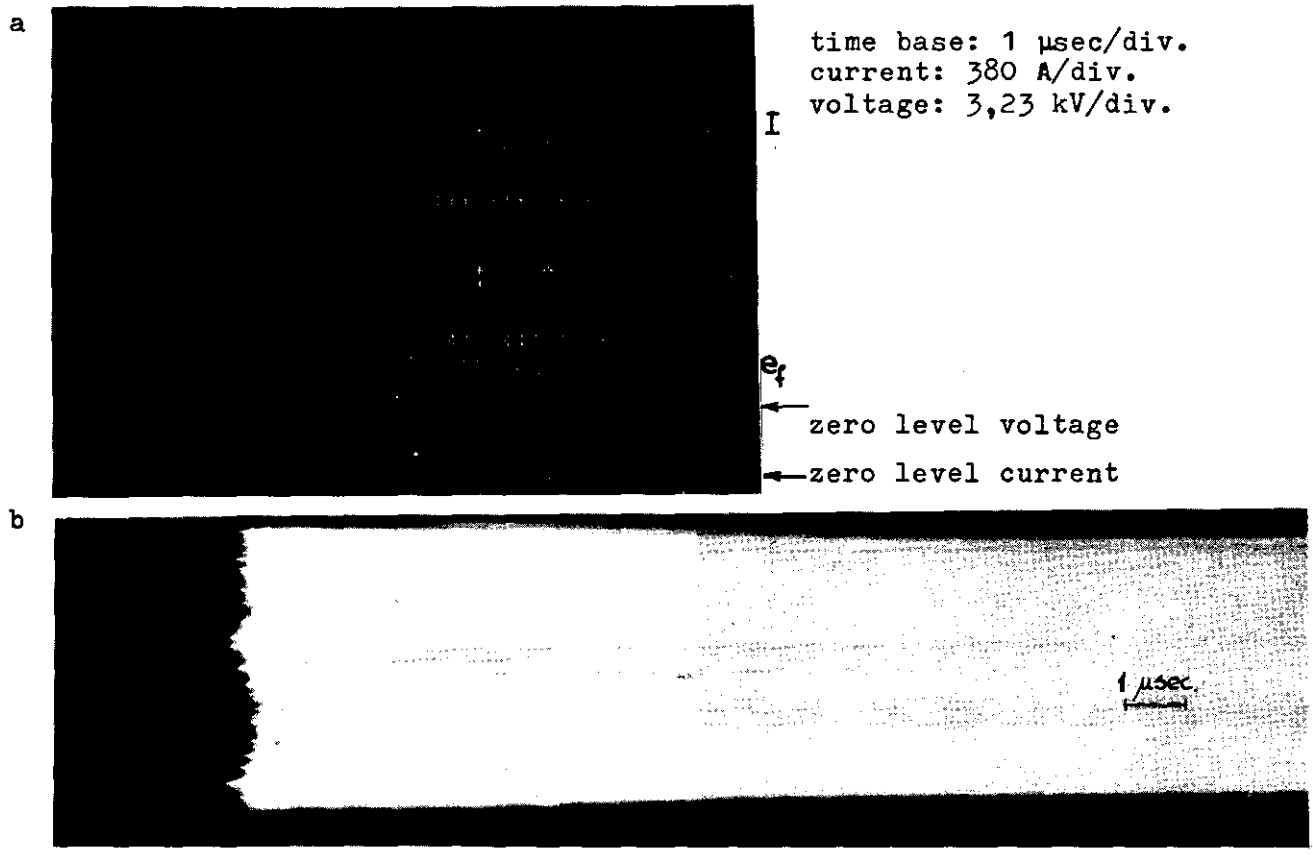

Fig. 3.5.2. Fusing silver wire 0.15 mm ø, 7 cm length.
Current value at the onset of the discharge: 1640 A.

are clearly visible. The streak record was made with the wire placed parallel to the slit opening, so the wire was filmed over its whole length. In this way it can be observed on which spots and at which time, local arcing occurs.
The instant a local arc starts can be observed in the voltage trace. The initiation of such a discharge is characterised by a little voltage step on the oscillogram. As soon as the arc has been established, the voltage drops until a new arc commences.
Irregularities in wire diameter cause varying current densities and a quicker heating at the smaller cross-sections. This process is particularly dependent on the surface tension of the material [15]. On spots where irregularities occur, small arcs appear immediately after local evaporation of the wire.
Similar experiments have been carried out with a higher value of the current. It is shown that the phenomena just described, disappear.
Fig. 3.5.2 shows streak records taken under the same conditions as used for fig. 3.5.1 but applying a higher current. It can be seen that local arcing happens to a far less extent.
Arcs appear at almost the same instant and are restricted to a very short interval. The shape of the voltage peak is more pronounced, its slope smoother with fewer disturbances. In other words, the expansion of the wire is uniform when the voltage has a smooth slope to the peak value without the irregularities of fig. 3.5.1.

Further investigations proved that the uniform expansion of the wire not only depends on a minimum value of the current, but that also the condition of the wire itself has to be taken into account. When exposed to polluted air, the wire surface adsorbs gases and corrodes. The influence of the corrosion layer manisfests itself in local arcing and irregular voltage traces, occurring even on a current level where these phenomena are not expected. Experiments with wires free from corrosion did not, or to a far less extent, show these effects (Holström et al. [20] show the influence caused by an impurity layer, on voltage-current traces and X-ray output, when evaporation of a tungsten wire is completed).
Fig. 3.5.3 illustrates again the difference in the voltage trace. The two experiments were performed under the same recording circumstances. Fig. 3.5.3a was taken with a "clean" wire submitted to a current whose level lies above the minimum. No irregularities can be seen, except the

transients in current and voltage, which we ascribe to circuit disturbances.
For fig. 3.5.3b a wire of the same diameter was used, which had been exposed to air for a certain time. The value of the voltage peak is much lower and not so pronounced, while its slope is more irregular. Fig. 3.5.4 shows the deviations occurring when both phenomena, i.e. minimum value of the current and corrosion, play an important role.

It is clear that these effects should be eliminated in order to get reproducible measurements. Experiments carried out under identical circumstances and using wires with no visible corrosion layer gave considerable improvement. Deviations, however, still occurred and can be large in the area of the voltage peak. These deviations are presumably due to the fact that the wires were not sufficiently cleaned; thus corrosion and absorbed gases still have some influence.

Another fact which may account for the deviations in our experiments, is the way the wires are handled during mounting. Silver is a soft material and very ductile. Wires of small cross-sections become easily elongated and kinks rapidly occur. This, possibly combined with being not corrosion-free, could enhance the deviations, as experiments done with wires of 0.1 mm in diameter show.
For this reason this type of wire is not used for calculations.

Summarising, it can be stated that best results were obtained with wires of a minimum diameter of 0.15 mm, having a clean surface and being carefully mounted. In order to improve accuracy, several tests have been done under identical circumstances.

a

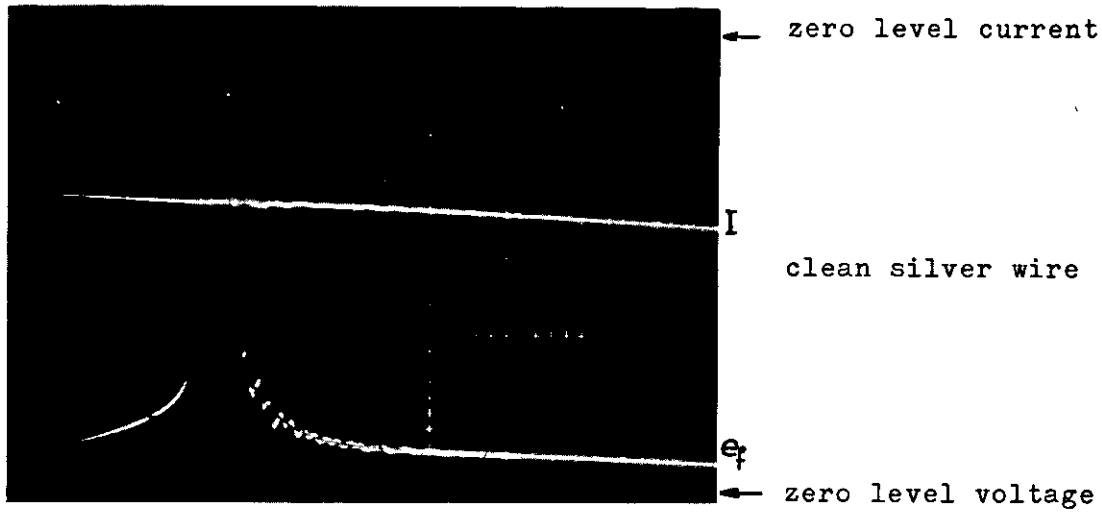

b

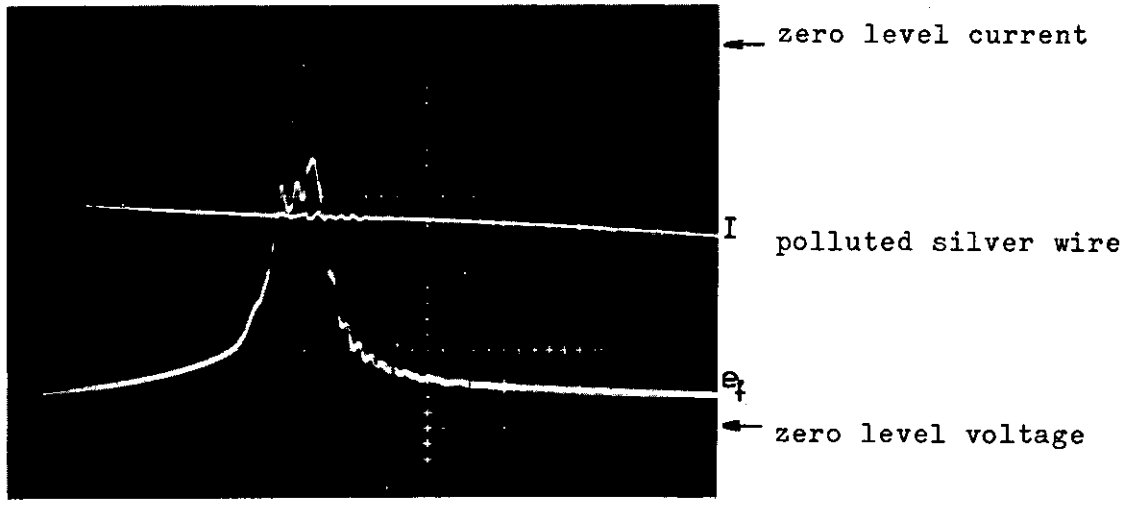

Fig. 3.5.3. Fusing silver wires 0.15 mm ø, 7 cm length.
Time base: 1 µsec/div; current: 760 A/div.
Voltage: 2900 V/div.

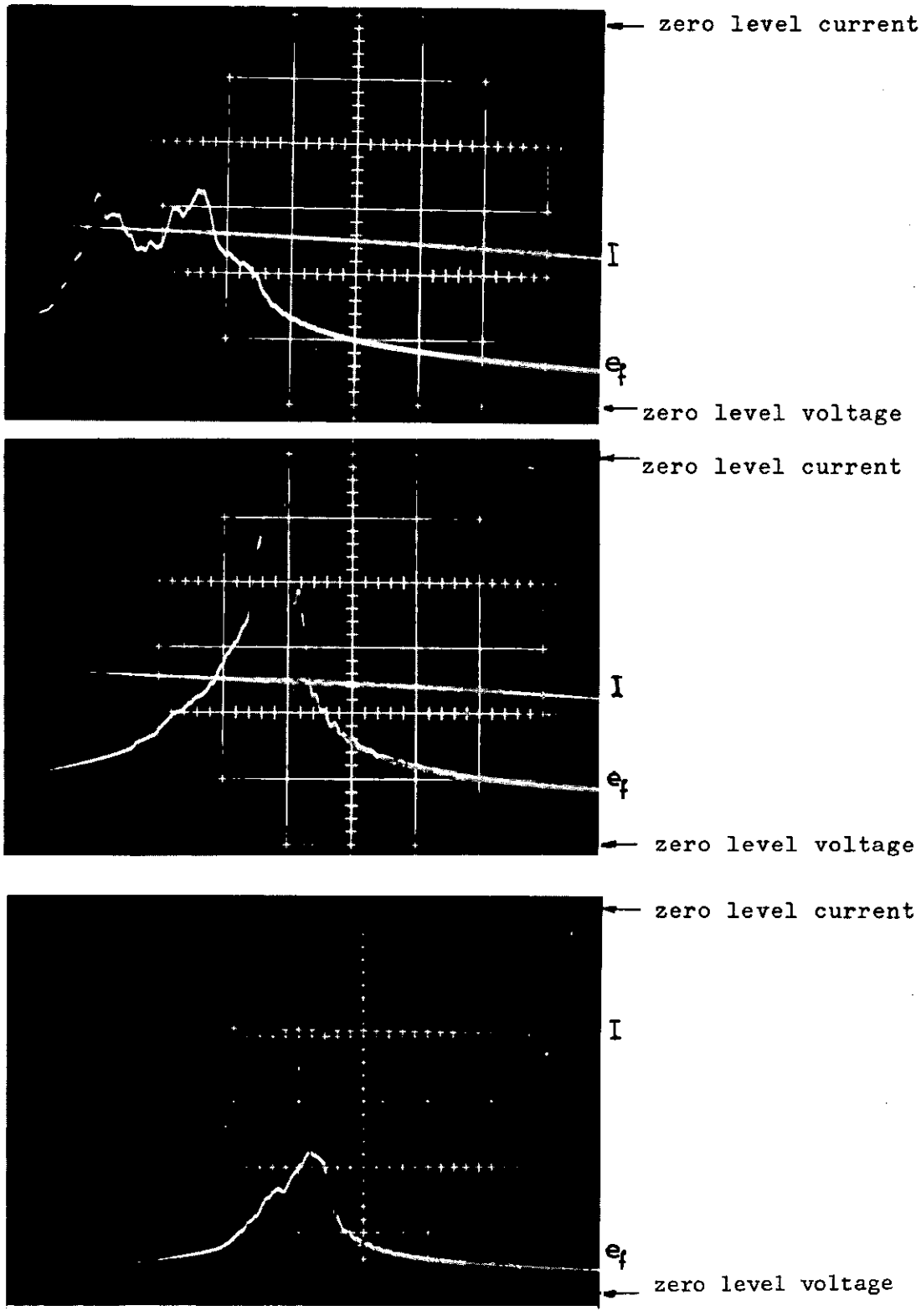

Fig. 3.5.4. Fusing silver wires 0,15 mm ⌀, 7 cm length.
Time base: 1 µsec/div.; current: 380 A/div.
Voltage: 1160 V/div.

4. Calculations and evaluation of the experiments

4.1. Introduction

In chapter 1 an energy balance was derived in the form of (2.1.5). The results obtained by experiment can now be used to discuss this expression.

Fig. 3.3.5 shows that during the first period (up to about 2 microsec.) after the onset of the discharge (see fig. 3.4.4, time t_4) the diameter-time dependency can be taken as linear, thus $d = d_o(1+\gamma t)$, d_o being the initial diameter of the discharge, and γ a time constant. The cross-section of the discharge can then be written

$$A = A_o(1+\gamma t)^2 = \tfrac{1}{4}\pi d_o^2(1+\gamma t)^2 \qquad (4.1.1)$$

Moreover it can be shown that the term $\frac{I_o^2 \cdot 10^{-7}}{2A}$ in equation (2.2.16) can be neglected with respect to $\frac{1}{A}\frac{dA}{dt}$. To justify this, (2.2.16) will be written

$$\Delta p = \left[\frac{1}{\alpha_1}\frac{1}{A}\frac{dA}{dt}\right]^2 + \frac{I_o^2}{2A}\cdot 10^{-7}$$

Substituting (4.1.1), we obtain:

$$\Delta p = \frac{1}{\alpha_1^2}\frac{4\gamma^2}{(1+\gamma t)^2} + \frac{I_o^2 \cdot 10^{-7}}{\frac{1}{2}\pi d_o^2(1+\gamma t)^2}$$

We have to show that

$$\frac{4\gamma^2}{\alpha_1^2} \gg \frac{I_o^2 \cdot 10^{-7}}{\frac{\pi}{2}\cdot d_o^2}$$

or: $2\pi\gamma^2 d_o^2 \cdot 10^7 \gg I_o^2 \alpha_1^2$

The factor γd_o represents the slope of the diameter-time curves. We notice that, for a given wire diameter, the slopes are all of the same order. It suffices, therefore, that for each wire diameter we take the case in which the slope angle is smallest and the current strongest. The results are shown in table 4.1.

Table 4.1

wire diameter	current	α_1	$2\pi\gamma^2 d_o^2 . 10^7$	$I_o^2 \alpha_1^2$
0.15 mm	2.12 kA	$6.7.10^2 kg^{-\frac{1}{2}} m^{\frac{1}{2}}$	$0.48.10^{15} m^2/sec^2$	$0.20.10^{13} m^2/sec^2$
0.20 mm	2.99 kA	$5.0.10^2 kg^{-\frac{1}{2}} m^{\frac{1}{2}}$	$1.30.10^{15} m^2/sec^2$	$0.22.10^{13} m^2/sec^2$

α_1 was calculated using the relation $\alpha_1 = \sqrt{\frac{8\pi}{M(Z+2)}}$
The charge number Z was taken = 1; the mass per metre M proved to be $18.6.10^{-6}$kg/m for a wire diameter of 0.15 mm and $33.0.10^{-6}$kg/m for 0.20 mm wire diameter.

Hence it is justified to replace (2.2.16) by the formula

$$\frac{1}{A}\frac{dA}{dt} = \alpha_1 \sqrt{\Delta p} \qquad (4.1.2)$$

Both (4.1.1) and (4.1.2) are now substituted in (2.1.5), and making use of (2.1.3) we obtain:

$$\frac{1}{\rho}\frac{d\rho}{dt} = \frac{1}{\alpha_2}\left[\frac{A_o 8\gamma^3}{\alpha_1^2}\frac{1}{1+\gamma t} - I^2 R_f\right]$$

Dividing by $I^2 R_{f_o}$ and using the relation $\frac{1}{1+\gamma t} = \sqrt{\frac{A_o}{A}}$ we obtain

$$\frac{\alpha_2}{I^2 R_{f_o} \rho}\frac{d\rho}{dt} = \lambda\sqrt{\frac{A_o}{A}} - \frac{R_f}{R_{f_o}} \qquad (4.1.3)$$

with

$$\lambda = \frac{1}{\alpha_1^2}\frac{A_o 8\gamma^3}{I^2 R_{f_o}}$$

The equation (4.1.3) comprises two important suppositions:
(1) The relation (4.1.2), theoretically derived, is correct;
(2) the cross-section of the discharge A is identical with the cross-section of the arc channel in which the current flows.
If the last assumption is true, it is allowed to compute the diameter of the current channel by using the data obtained from streak records.

For testing these suppositions for their validity, two experimental

facts not depending on each other are necessary. This information is supplied by calculating the specific resistance ρ and the slope of the ρ - T characteristic.

4.2. The relation $\alpha_1\sqrt{\Delta p} = \frac{1}{A}\frac{dA}{dt}$

Fig. 4.2.1 shows the resistance of the discharge as a function of time for a number of current values at which also streak records were taken. To compare the different results, the momentary value of the resistance is divided by the initial value the discharge has at the time of onset (fig. 3.4.1, t_4). The curves obtained are the average result of a number of measurements (see fig. 4.2.2; for a wire diameter of 0.10 mm, there is no clear relationship between voltage and fusing current for reasons explained earlier).

Knowing the resistance and the cross-section of the discharge as a function of time on a common time base, the specific resistance can be calculated using $R_f = \rho \cdot \frac{1}{A}$, R_f being the resistance of the plasma column, 1 the length of the wire (7 cm), and A the cross-section of the column. In fig. 4.2.3 the specific resistance is plotted against time for different current values and wire diameters. We notice that the slope of the function can become positive, negative or zero.

We first consider the case of $\frac{d\rho}{dt} = o$.
The energy equation (2.1.5) indicates that in this case $I^2R_f = \Delta p \frac{dA}{dt}$, i.e. the electrical input energy equals the expansion energy.
Using (4.1.3) by substituting $\frac{d\rho}{dt} = o$ in this equation we obtain:

$$\lambda\sqrt{\frac{A_o}{A}} = \frac{R_f}{R_{f_o}} \qquad (4.2.1)$$

To establish whether the experiments satisfy (4.2.1) for $\frac{d\rho}{dt} = o$, the factor λ was computed, A_o and R_{f_o} being the initial cross-section and resistance of the discharge. The terms $\frac{R_f}{R_{f_o}}$ and $\sqrt{\frac{A_o}{A}}$ are given by fig. 4.2.1 and fig. 3.3.5 at the times when $d\rho/dt = o$, obtained from fig. 4.2.3.

The results are collected in table 4.2.

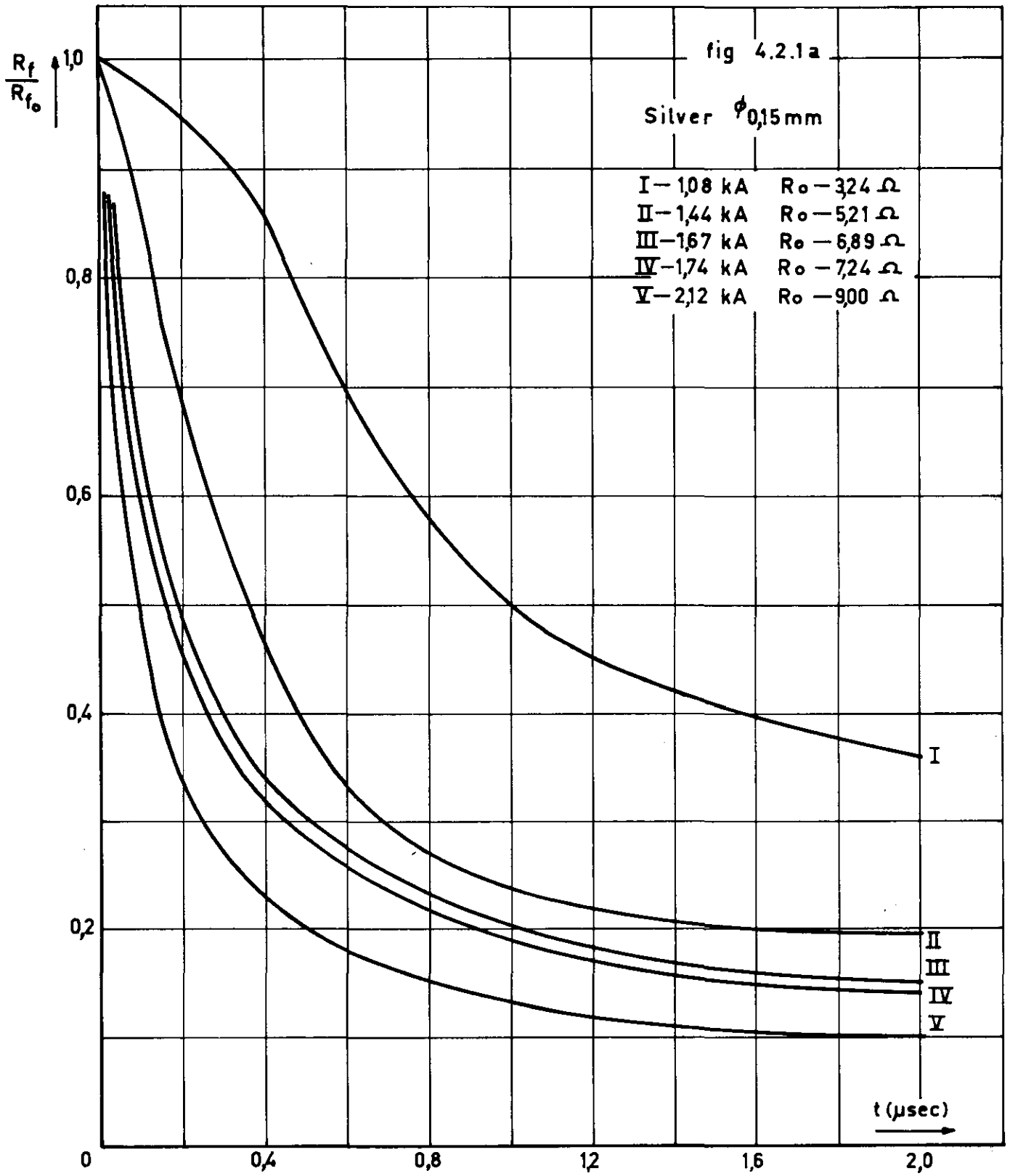
fig 4.2.1a
Silver ϕ 0,15mm
I – 1,08 kA Ro – 3,24 Ω
II – 1,44 kA Ro – 5,21 Ω
III – 1,67 kA Ro – 6,89 Ω
IV – 1,74 kA Ro – 7,24 Ω
V – 2,12 kA Ro – 9,00 Ω
$\frac{R_f}{R_{f_o}}$
1,0
0,8
0,6
0,4
0,2
0
0,4
0,8
1,2
1,6
2,0
t (μsec)
I
II
III
IV
V

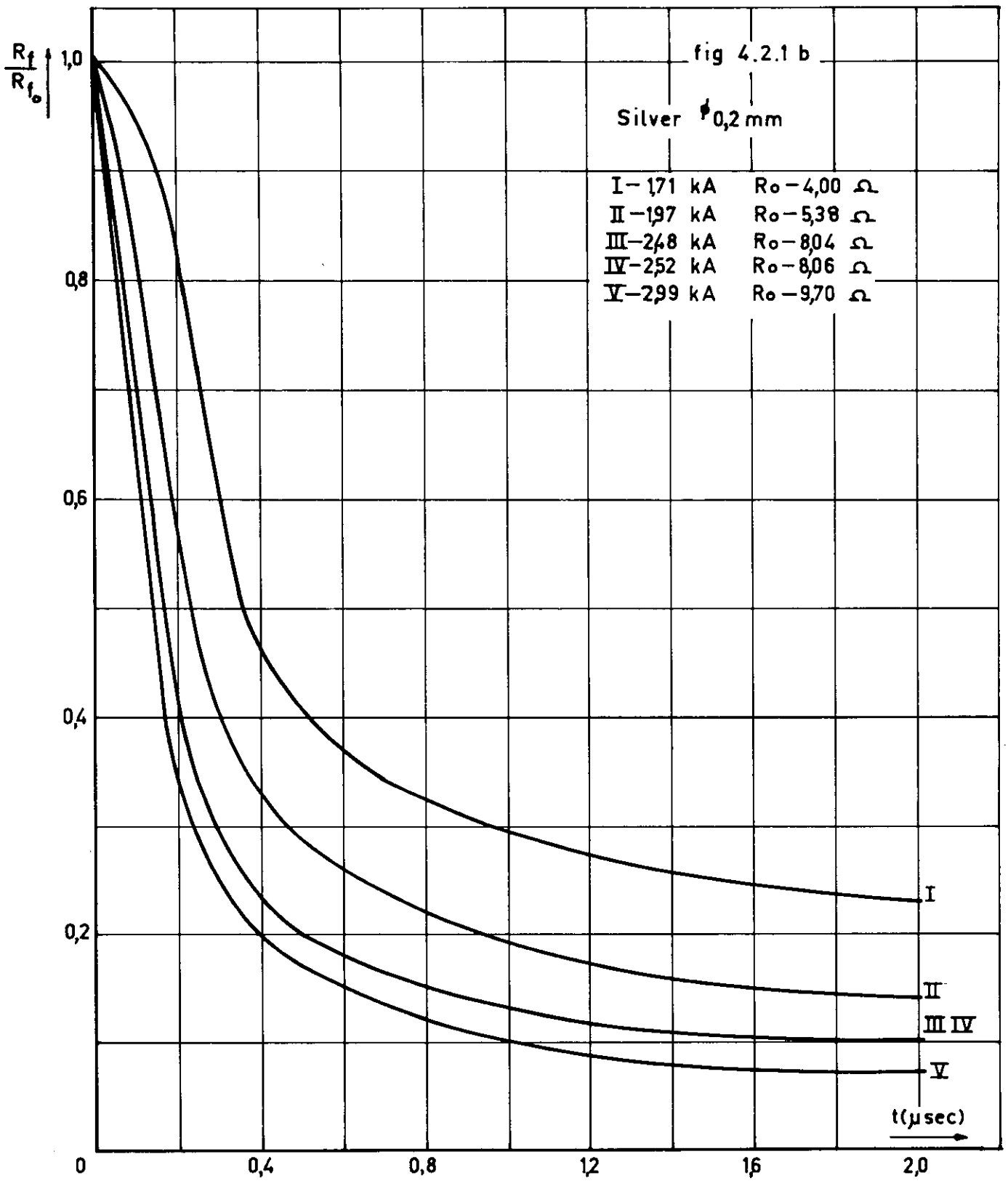
fig 4.2.1 b
Silver ϕ 0,2 mm
I – 1,71 kA Ro – 4,00 Ω
II – 1,97 kA Ro – 5,38 Ω
III – 2,48 kA Ro – 8,04 Ω
IV – 2,52 kA Ro – 8,06 Ω
V – 2,99 kA Ro – 9,70 Ω
Rf / Rfo
1,0
0,8
0,6
0,4
0,2
0
0,4
0,8
1,2
1,6
2,0
t(μsec)
I
II
III IV
V

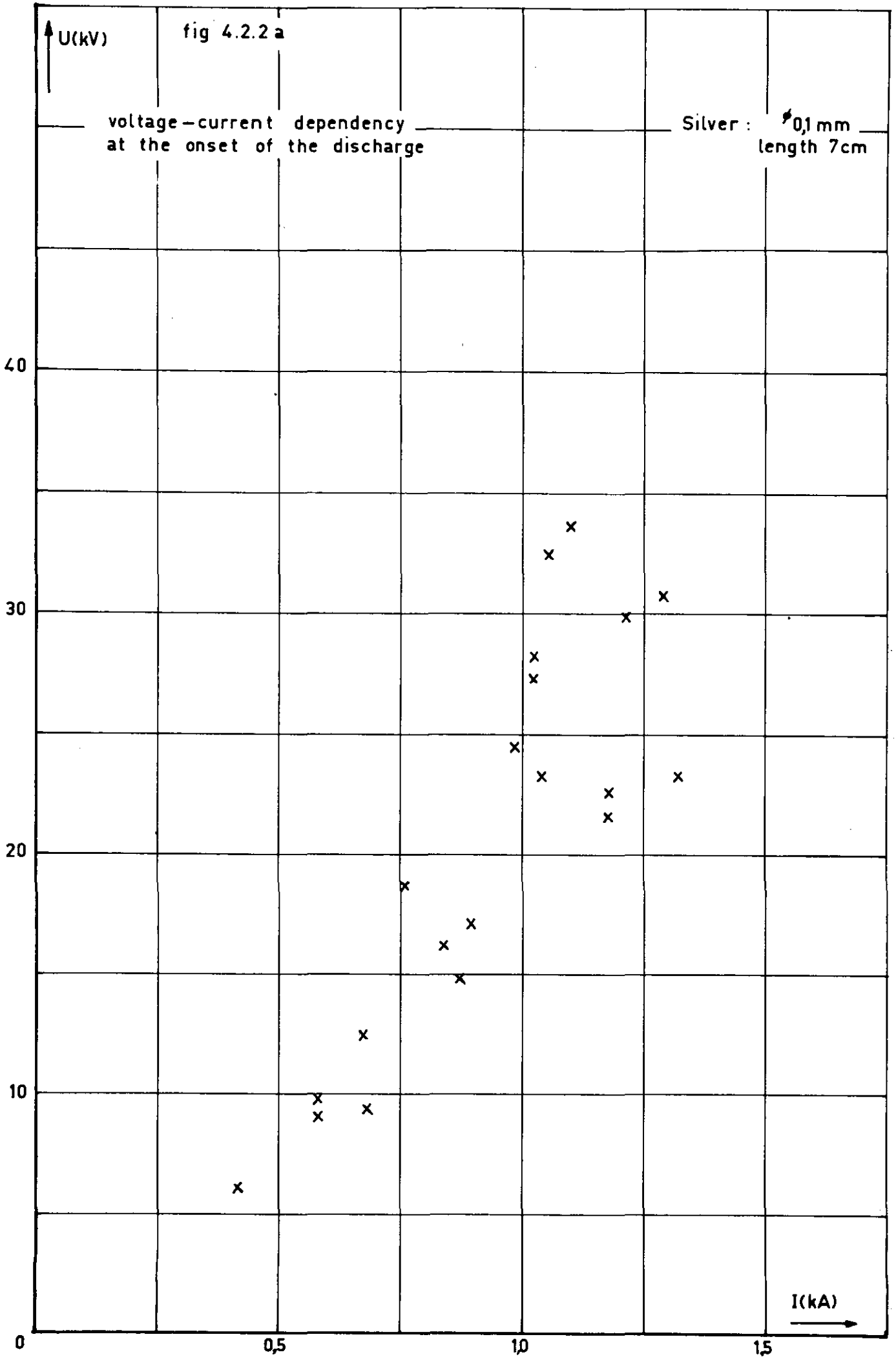
U(kV)
fig 4.2.2 a
voltage – current dependency
at the onset of the discharge
Silver : ϕ 0,1 mm
length 7cm
40
30
20
10
0
0,5
1,0
1,5
I(kA)

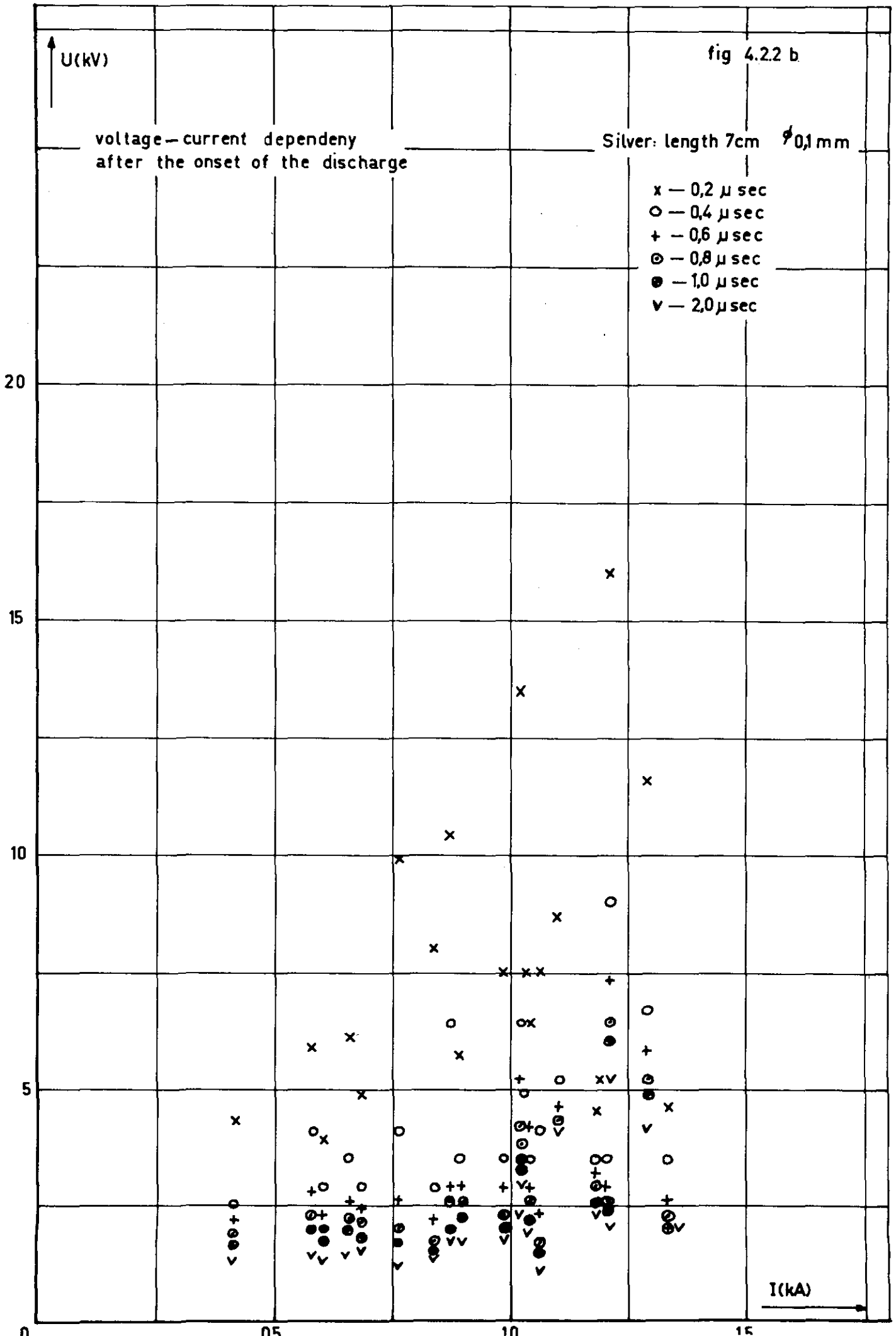
U(kV)
fig 4.2.2 b
voltage – current dependeny
after the onset of the discharge
Silver: length 7cm ϕ 0,1 mm
x — 0,2 μ sec
o — 0,4 μ sec
+ — 0,6 μ sec
⊙ — 0,8 μ sec
● — 1,0 μ sec
v — 2,0 μ sec
20
15
10
5
0
05
10
15
I(kA)

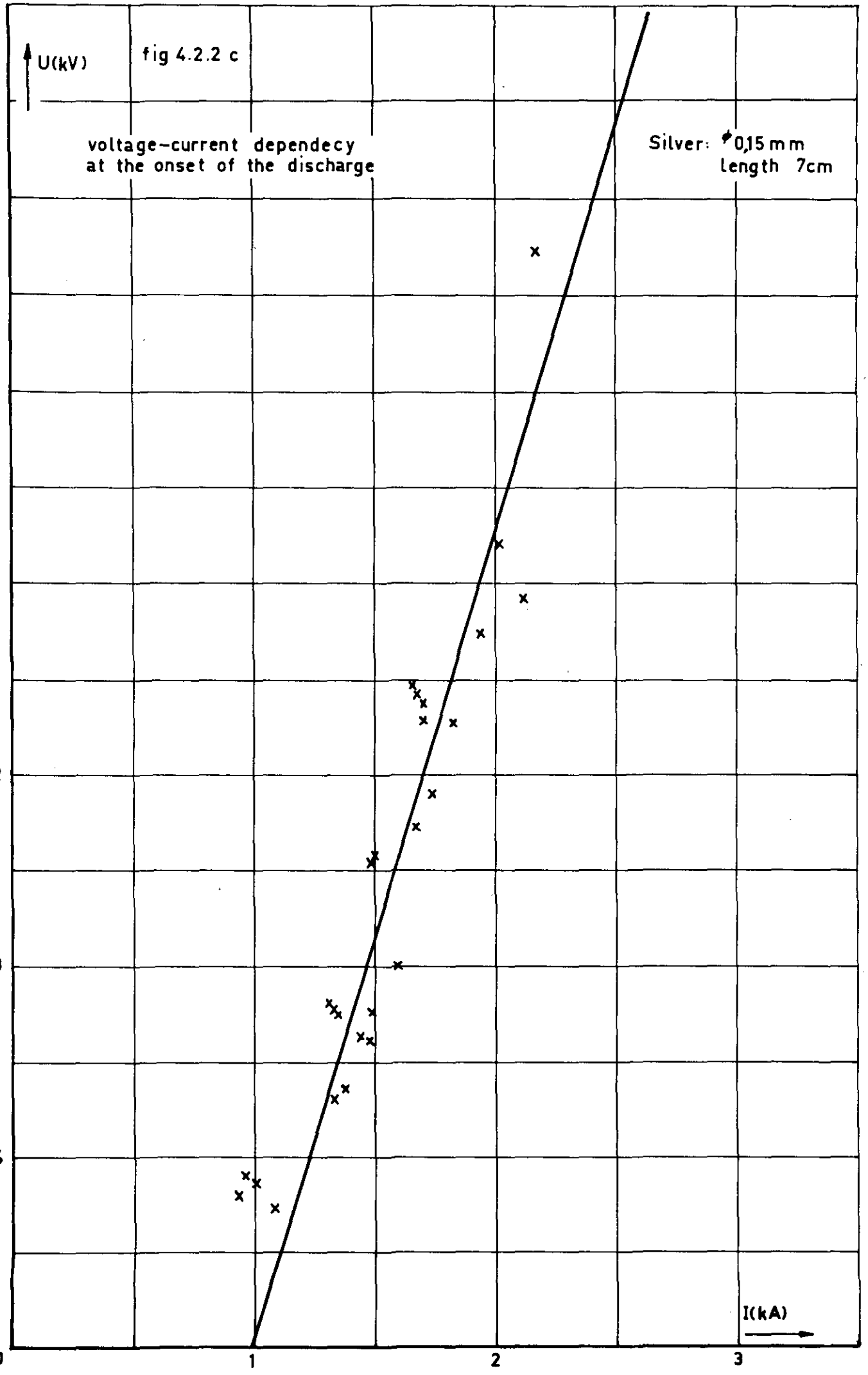
U(kV)
fig 4.2.2 c
voltage-current dependecy
at the onset of the discharge
Silver: ϕ 0,15 mm
length 7cm
24
20
16
12
8
4
0
1
2
3
I(kA)

fig 4.2.2 d

voltage-current dependency
after the onset of the discharge

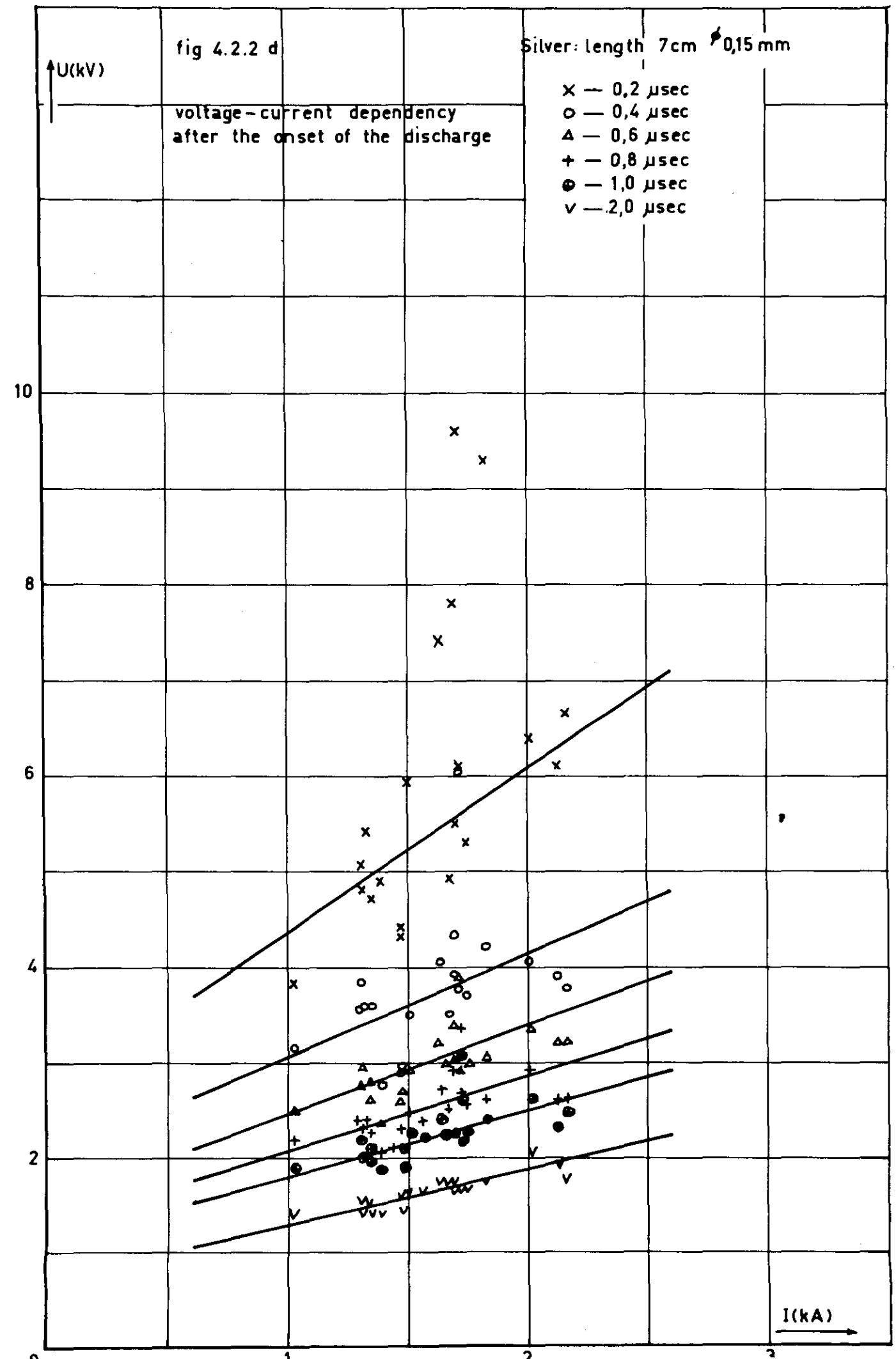

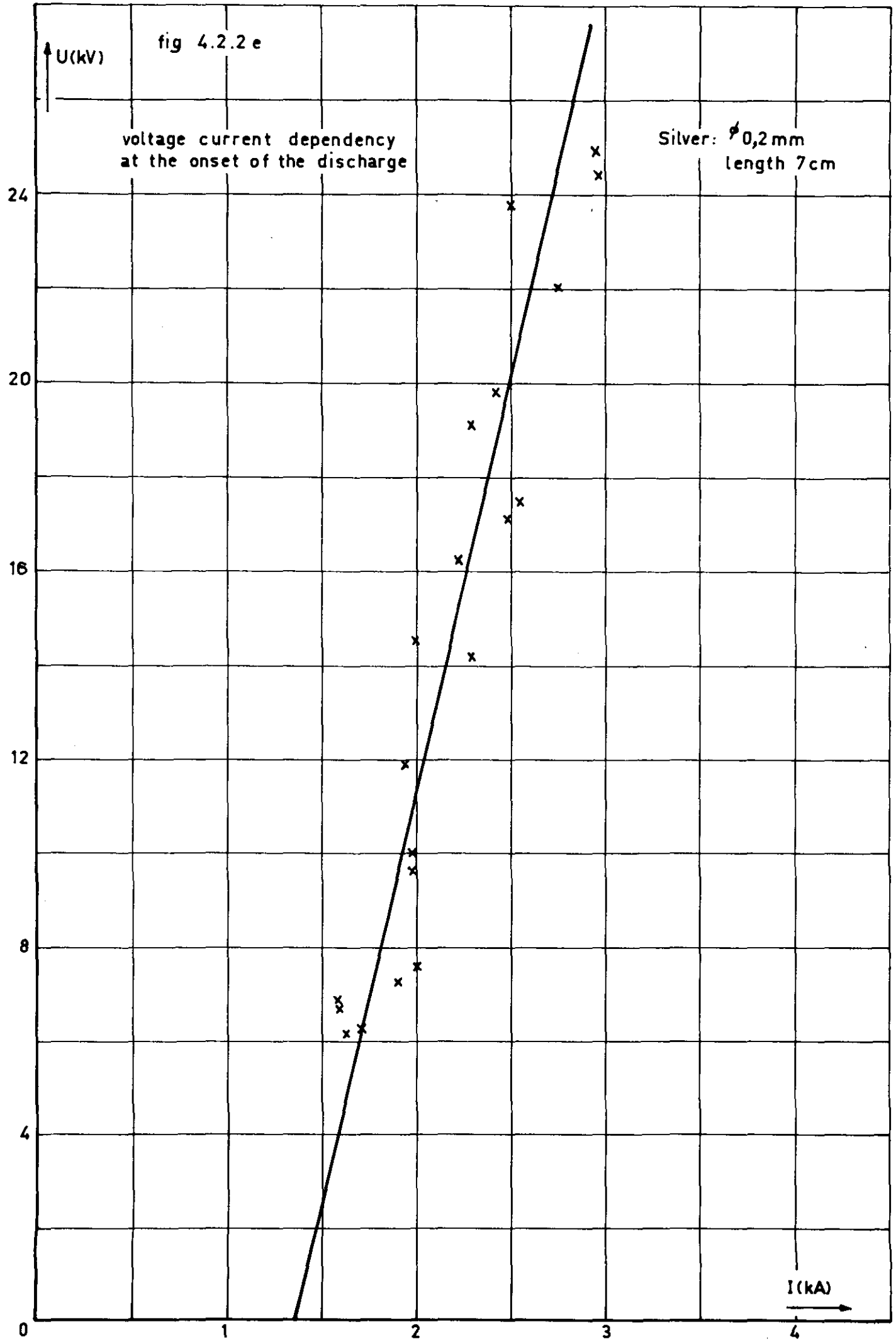
U(kV)
fig 4.2.2 e
voltage current dependency
at the onset of the discharge
Silver: ϕ 0,2 mm
length 7 cm
24
20
16
12
8
4
0
1
2
3
4
I(kA)

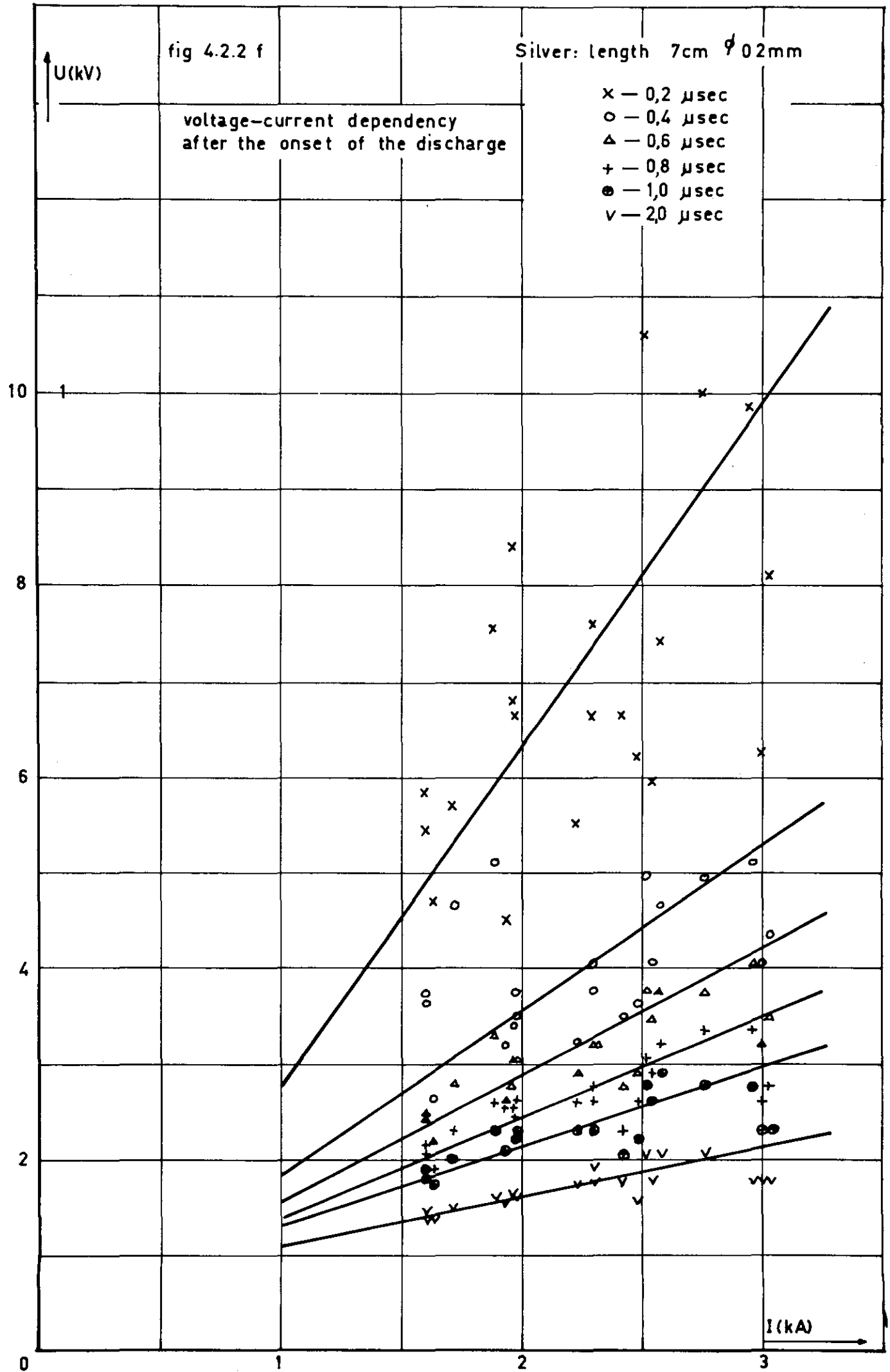
fig 4.2.2 f
U(kV)
voltage–current dependency
after the onset of the discharge
Silver: length 7cm ϕ 0,2mm
× — 0,2 µsec
○ — 0,4 µsec
△ — 0,6 µsec
+ — 0,8 µsec
⊕ — 1,0 µsec
v — 2,0 µsec
10
8
6
4
2
0
1
2
3
I (kA)

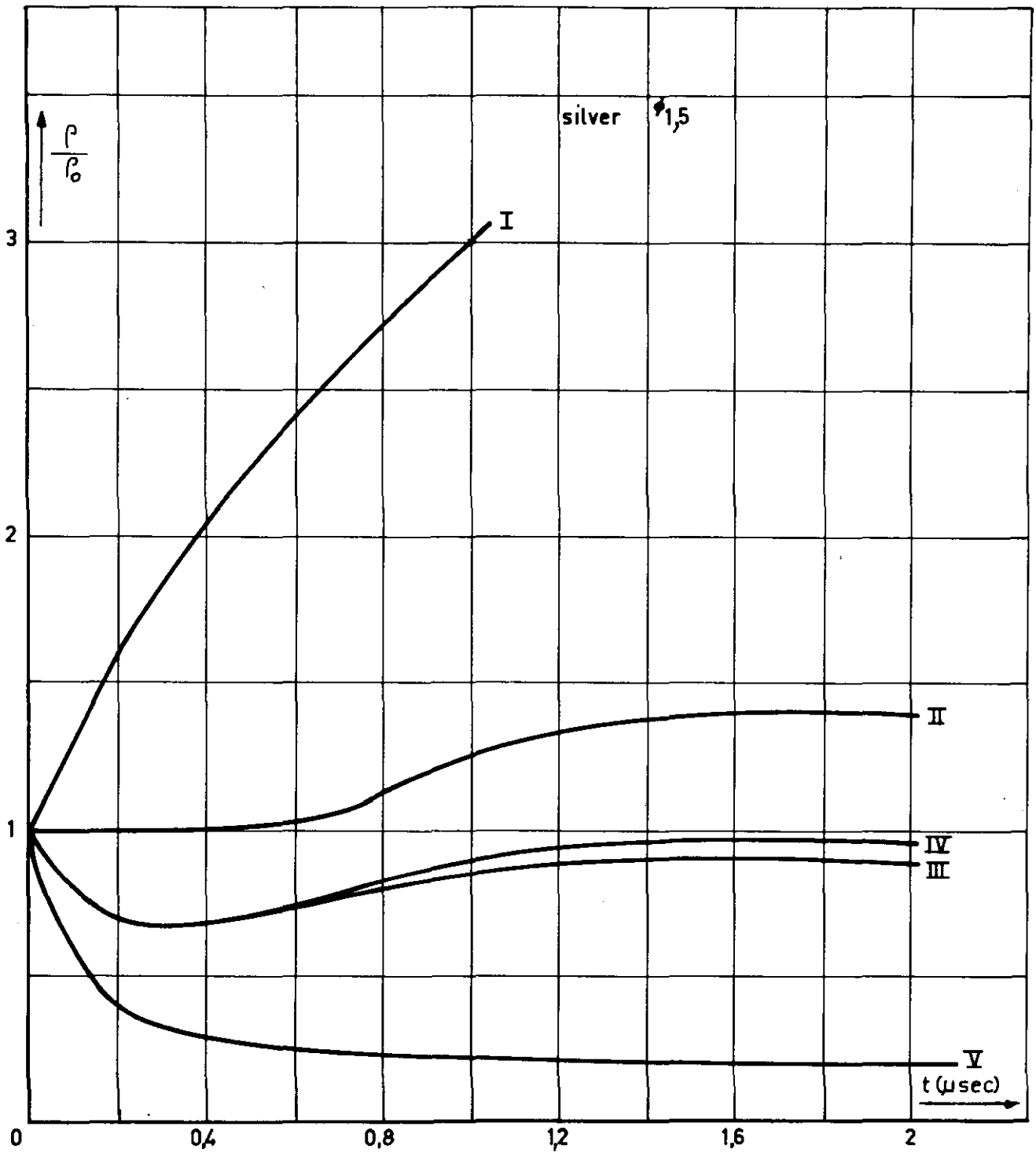

I 1,08 kA $\rho_0 = 1{,}25 \times 10^{-4}$ Ω m
II 1,44 kA $\rho_0 = 3{,}50 \times 10^{-4}$ Ω m
III 1,67 kA $\rho_0 = 6{,}05 \times 10^{-4}$ Ω m
IV 1,74 kA $\rho_0 = 6{,}36 \times 10^{-4}$ Ω m
V 2,12 kA $\rho_0 = 1{,}86 \times 10^{-3}$ Ω m

fig 4.2.3 b

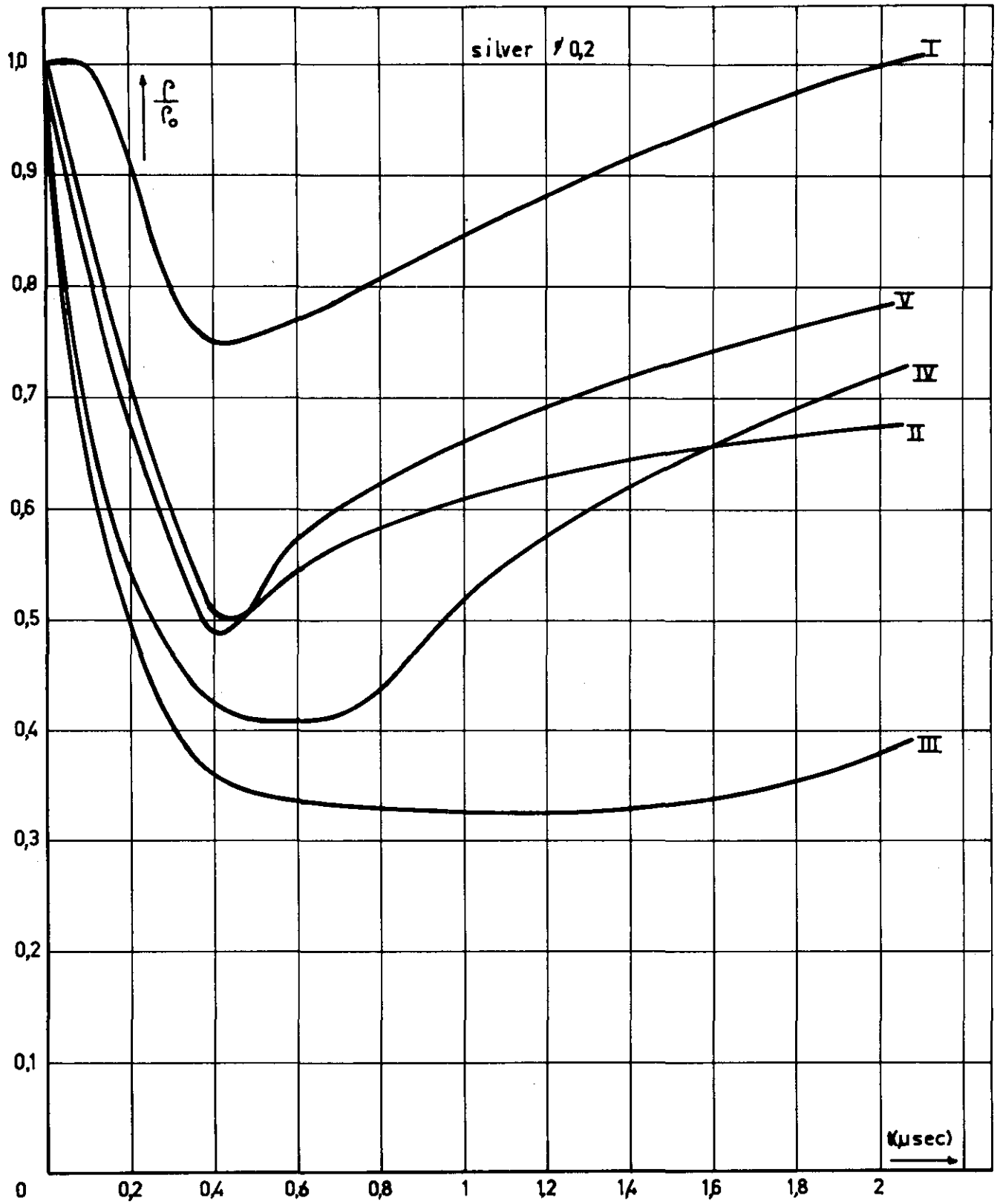

I 1,71 kA $\rho_0 = 5{,}20 \times 10^{-4}$ Ω m

II 1,97 kA $\rho_0 = 8{,}26 \times 10^{-4}$ Ω m

III 2,48 kA $\rho_0 = 1{,}17 \times 10^{-3}$ Ω m

IV 2,52 kA $\rho_0 = 1{,}87 \times 10^{-3}$ Ω m

V 2,99 kA $\rho_0 = 8{,}50 \times 10^{-4}$ Ω m

Table 4.2

	I kA	$t\left[\frac{d\rho}{dt}=o\right]^*$ μsec	R_{f_o} $10^2\Omega$	λ	$\sqrt{\frac{A_o}{A}}$	$\lambda\sqrt{\frac{A_o}{A}}$	$\frac{R_f}{R_{f_o}}$
d=0.15mm	1.44	0.0	0.74	0.78	1.00	0.78	1.00
		0.2	0.74	0.78	0.81	0.63	0.68
		0.4	0.74	0.78	0.68	0.53	0.48
	1.67	0.3	0.98	0.40	0.76	0.34	0.40
		2.0	0.98	0.40	0.40	0.16	0.15
	1.74	0.3	1.03	0.35	0.74	0.27	0.43
		2.0	1.03	0.35	0.39	0.14	0.14
	2.12	1.0	1.29	0.12	0.80	0.10	0.14
		2.0	1.29	0.12	0.72	0.10	0.10
d=0.20mm	1.71	0.0	0.57	1.28	1.00	1.28	1.00
		0.4	0.57	1.28	0.79	1.00	0.45
	1.97	0.45	0.77	0.73	0.75	0.54	0.30
	2.48	0.8	1.15	0.28	0.67	0.19	0.15
		1.0	1.15	0.28	0.63	0.17	0.13
	2.52	0.6	1.15	0.22	0.66	0.15	0.17
	2.99	0.4	1.39	0.77	0.61	0.47	0.20

Comparing the values of $\lambda\sqrt{\frac{A_o}{A}}$ and $\frac{R_f}{R_{f_o}}$ (fig. 4.2.4), we see that there is fair agreement. Especially the values for a wire diameter of 0.15 mm differ only very little. The discrepancies for 0.20 mm are somewhat larger. Considering the accuracy which can be reached by the measurements and the assumptions made, we may conclude that the result is reasonable.

As will be noticed, relation (4.2.1) consists of terms which can be measured directly, except $\alpha_1 = \sqrt{\frac{8\pi}{M(Z+2)}}$. The total mass per metre M is not likely to change during the process. The boundaries available for computing the diameter of the discharge, are defined very sharply. The velocities, attained by the plasma show that its boundaries can be seen as being shock fronts; transport of mass over these boundaries will therefore be very small, if not negligible.

* the time t=o coincides with the time t_4 in fig. 3.4.1.

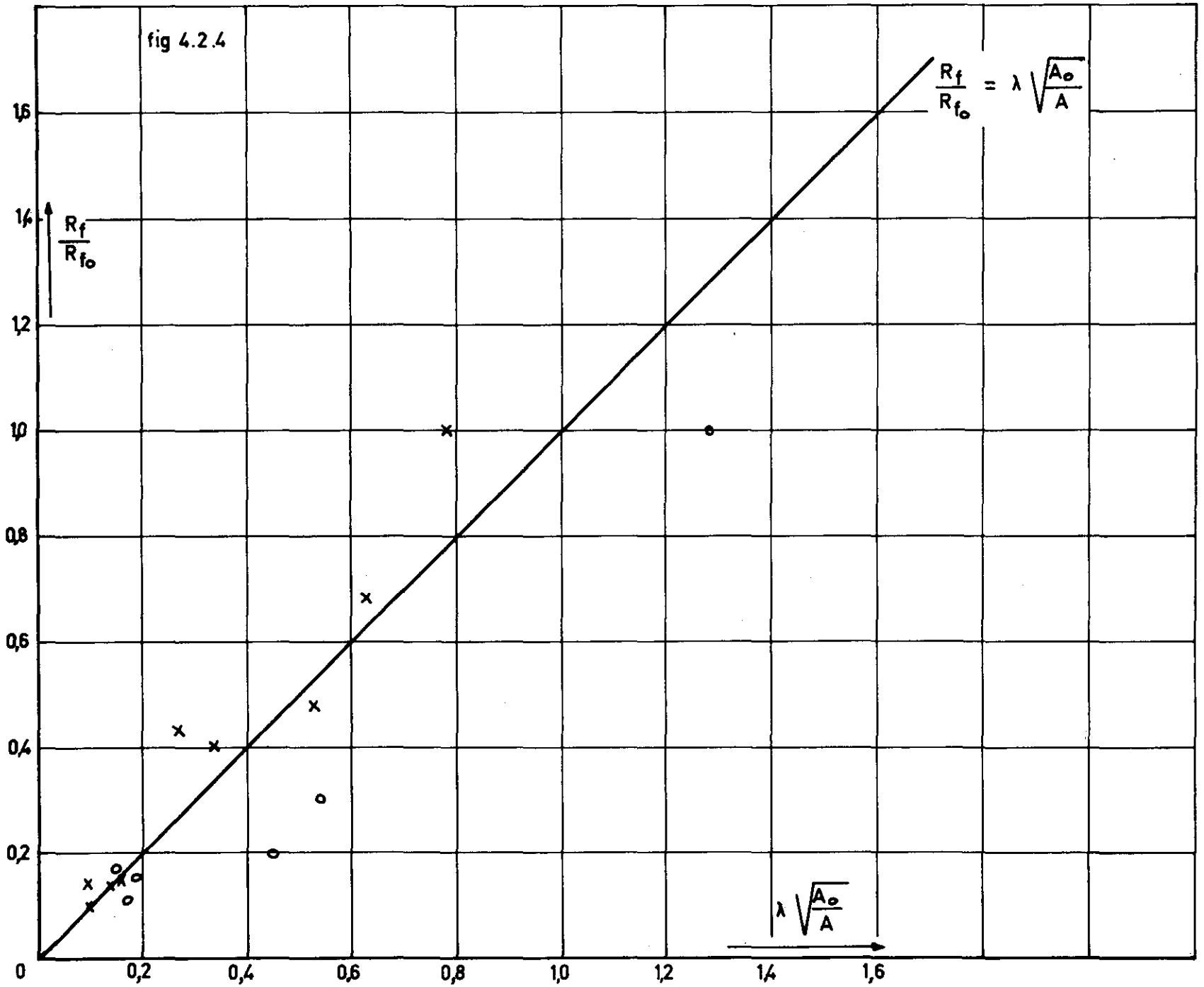
fig 4.2.4
$\frac{R_f}{R_{fo}} = \lambda \sqrt{\frac{A_o}{A}}$
$\frac{R_f}{R_{fo}}$
$\lambda \sqrt{\frac{A_o}{A}}$
0
0,2
0,4
0,6
0,8
1,0
1,2
1,4
1,6

The same applies to the charge number Z. The silver vapour is fully ionised for temperatures beyond 10^4 °K, and pressures ranging from 1 - 50 atmospheres [1]. Values of ρ obtained by experiment are roughly between $10^{-3}\Omega$m and $10^{-4}\Omega$m, indicating temperatures from 7000°K up to 14,000°K (see fig. 2.1). In this region it is likely that Z = 1 will not alter appreciably.
So we may expect that α_1 can be considered to be a constant during the whole process.

Our starting point was that if the specific resistance remains a constant during a certain time, the electrical energy must equal the expansion energy: $I^2R_f = \Delta p \frac{dA}{dt}$. We have shown that the equation $\lambda\sqrt{\frac{A_o}{A}} = \frac{R_f}{R_{f_o}}$ holds with a certain accuracy. This means that the relation (4.1.2), i.e. our first assumption made above, is justified.

4.3. The signs of the terms in the energy equation

We now inquire the situations in which the slope of the specific resistance is unequal to zero. From eq. (2.1.5) it follows that:

(1) $\frac{d\rho}{dt} < o$ if $I_f^2R_f > \Delta p \frac{dA}{dt}$; the input energy exceeds the expansion energy, the plasma is heated, and the temperature increases, which causes the specific resistance to drop;

(2) $\frac{d\rho}{dt} > o$ if $I_f^2R_f < \Delta p \frac{dA}{dt}$; the expansion energy is larger than the electrical energy. This results in a temperature decrease and accordingly an increase in the specific resistance.

Using (4.1.3), it can be investigated whether these inequalities hold. We have to show that:

(1) if $\frac{d\rho}{dt} > o$ $\qquad \lambda\sqrt{\frac{A_o}{A}} - \frac{R_f}{R_{f_o}} > o$

(2) if $\frac{d\rho}{dt} < o$ $\qquad \lambda\sqrt{\frac{A_o}{A}} - \frac{R_f}{R_{f_o}} < o$

We have computed these terms in table 4.3.

Table 4.3

$$\lambda \sqrt{\frac{A_o}{A}} - \frac{R_f}{R_{f_o}}$$

wire diameter 0.15 mm

I time kA μsec	0.0	0.2	0.4	0.6	0.8	1.0	2.0
2.12	-0.88	-0.22	-0.12	-0.09	-0.05	-0.04	-0.02
1.74	-0.65	-0.19	-0.08	-0.05	-0.04	-0.03	-0.02
1.67	-0.60	-0.16	-0.05	-0.03	-0.02	-0.01	0.01
1.44	-0.20	-0.02	0.08	0.10	0.10	0.10	0.10
1.08	2.02	1.39	1.07	0.94	0.81	0.74	
			$10^2 \cdot \frac{1}{I^2 R_{f_o} \rho} \frac{d\rho}{dt}$				
2.12	-1.69	-0.35	-0.18	-0.11	-0.07	0.00	0.00
1.74	-1.11	-0.20	0.05	0.16	0.13	0.13	0.02
1.67	-1.28	-0.23	0.06	0.18	0.11	0.11	0.00
1.44	0.00	0.00	0.00	0.07	0.21	0.21	0.00
1.08	5.56	2.93	1.74	1.20	0.93	0.93	

$$\lambda \sqrt{\frac{A_o}{A}} - \frac{R_f}{R_{f_o}}$$

wire diameter 0.20 mm

I time kA µsec	0.0	0.2	0.4	0.6	0.8	1.0	2.0
2.99	0.32	0.15	0.24	0.20	0.18	0.17	0.14
2.52	-0.78	-0.21	-0.06	-0.02	-0.01	0.01	0.01
2.49	-0.72	-0.16	-0.01	0.00	0.01	0.01	0.01
1.97	-0.35	0.00	0.20	0.20	0.18	0.17	0.16
1.71	0.28	0.28	0.53	0.51	0.51	0.45	0.39
				$10^2 \cdot \frac{1}{I_f^2 R_{f_o} \rho} \frac{d\rho}{dt}$			
2.99	-0.17	-0.15	0.00	0.05	0.03	0.02	0.01
2.52	-0.82	-0.24	-0.07	0.00	0.09	0.08	0.03
2.49	-0.84	-0.29	-0.17	-0.03	-0.01	0.01	0.05
1.97	-0.40	-0.63	-0.50	0.19	0.11	0.07	0.00
1.71	0.00	-0.78	0.00	0.11	0.16	0.13	0.07

We now compare the signs of the expression $\lambda \sqrt{\frac{A_o}{A}} - \frac{R_f}{R_{f_o}}$, and $\frac{1}{\rho} \frac{d\rho}{dt}$ (see fig. 4.3.1).

For the majority of the values calculated (over 70%), both terms have the same sign; for those whose signs are different (underlined in the table) the difference between expansion energy and electrical energy is mostly small. The influence of errors will then be relatively large, which can cause a sign shift.

Our conclusion may be: as far as the signs of the different terms are concerned, our results are in reasonable agreement with the conditions, stated by the energy balance.

4.4. Calculation of the slope β of the ρ-T characteristic

In the conclusions previously made, the factor α_2 did not play a role. It was shown that relation (4.1.2) was satisfied. Furthermore the signs of the different terms in the energy balance proved to be in agreement with each other.

These facts are sufficient to use the energy balance in the form of (4.3.1) for calculating the value of α_2, and thereby the slope β of the ρ - T characteristic.

As has been mentioned, the values of ρ are between $10^{-3}\,\Omega$ m and $10^{-4}\,\Omega$ m. Fig. 2.1 shows that β can be subject to changes in these surroundings and cannot be taken as a constant.

From (4.1.3) we obtain the following expression for β:

$$\beta = C \frac{\frac{1}{I^2 R_{f_o} \rho} \frac{d\rho}{dt}}{\lambda \sqrt{\frac{A_o}{A} - \frac{R_f}{R_{f_o}}}} \qquad (4.4.1)$$

The heat capacity of the wire considered per metre was calculated, using the expression: $C = Mc_v$; M being the mass of the wire per metre; c_v, the specific heat per unit mass, was found using the relation $c_v = \frac{3}{2}kN$, where N is the total number of particles per unit mass, k is Boltzmann's constant it proved to be 115 J/°K.kg.

For a wire diameter of 0.15 mm C was found to be $2.13.10^{-3}$ J/°K.m; for 0.20 mm diameter $3.80.10^{-3}$ J/°K.m.

Table 4.4 shows a number of values of ρ.

fig 4.3.1

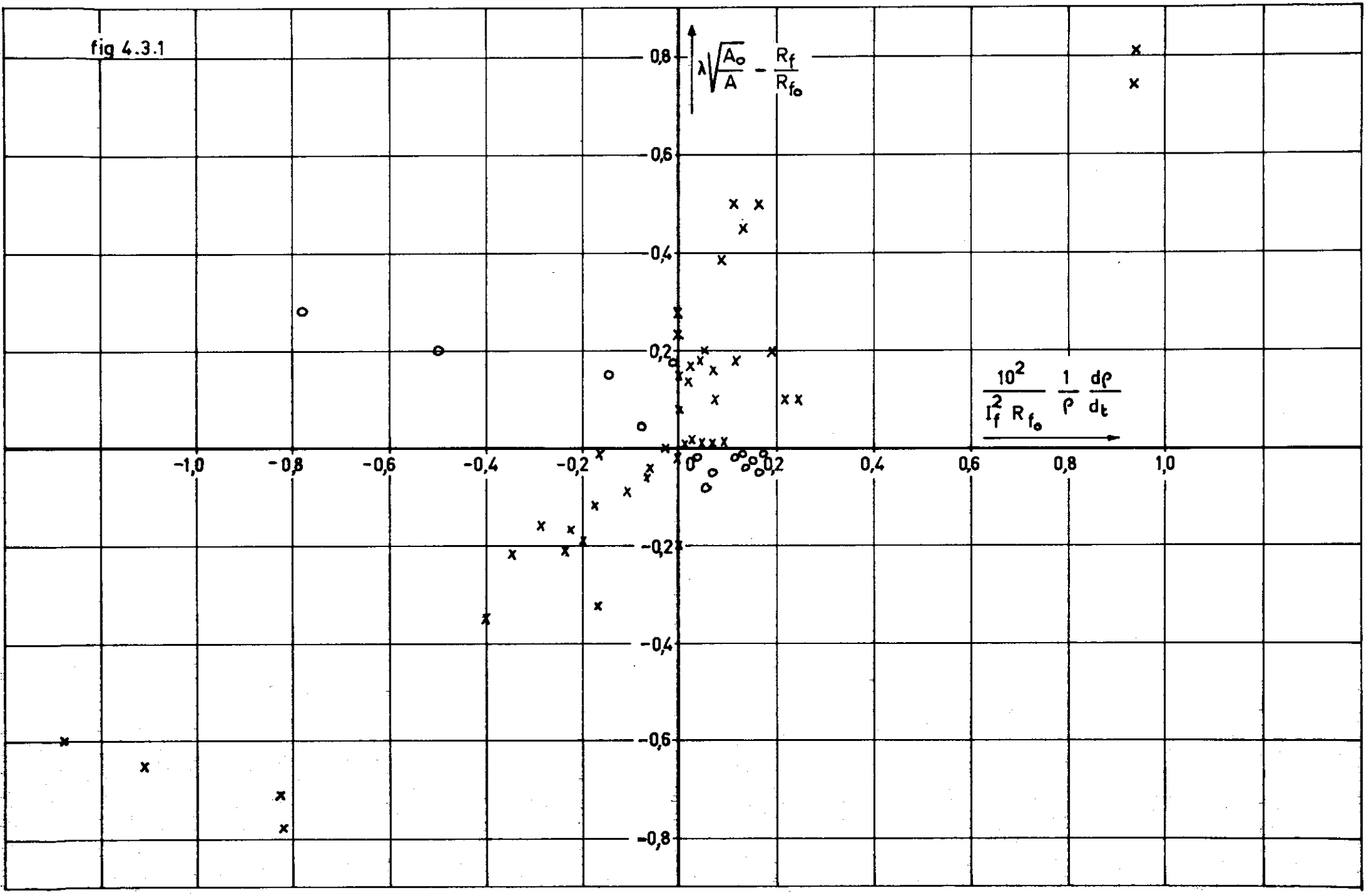
$\lambda\sqrt{\frac{A_o}{A}} - \frac{R_f}{R_{f_o}}$
$\frac{10^2}{I_f^2 R_{f_o}} \frac{1}{\rho} \frac{d\rho}{dt}$
0,8
0,6
0,4
0,2
-0,2
-0,4
-0,6
-0,8
-1,0
-0,8
-0,6
-0,4
-0,2
0,2
0,4
0,6
0,8
1,0

Table 4.4

$10^4 \beta$

d = 0.15 mm

I time kA µsec	0.0	0.2	0.4	0.6	0.8	1.0	2.0
2.12	4.1	3.4	3.3	2.8	2.7	0.0	0.0
1.74	3.6	2.3					
1.67	4.5	3.0					
1.44	0.0	0.0	0.0	1.6	4.8	4.5	0.0
1.08	5.9	4.5	3.5	2.7	2.6	2.7	
				$10^4 \beta$			
d = 0.20 mm							
2.99	2.0		0.0	1.0	0.6	0.4	0.3
2.52	4.0	4.3	4.3	0.0	60.0	45.5	20.3
2.49	4.4	6.9	45.5			2.5	13.3
1.97	4.4	709.5		3.7	2.3	1.5	0.0
1.71	0.0		0.0	0.9	1.2	1.6	0.7

Only those values have been calculated for which the condition of sign-agreement holds. Fig. 4.4.1 shows β as a function of the specific resistance ρ. The ρ-T characteristic can be approximated by three lines, having different values of β; see fig. 2.1b.

We now compare our results with this curve and make the following remarks:

(a) As can be seen we have found for some values that $\beta = 0$.
No physical meaning can be attached to this as this value appears when $\frac{d\rho}{dt}$ is about zero. We have shown that in the case of $\frac{d\rho}{dt} = 0$ the denominator of (4.4.1) should also be zero, which should mean theoretically that according to (4.4.1), β becomes indeterminable. The fact that nominator and denominator in (4.1.1) are not zero at the same time, is due to measuring errors. This results in β having either a value of zero or attaining a very large value.

(b) It has been mentioned that the values of ρ obtained are between

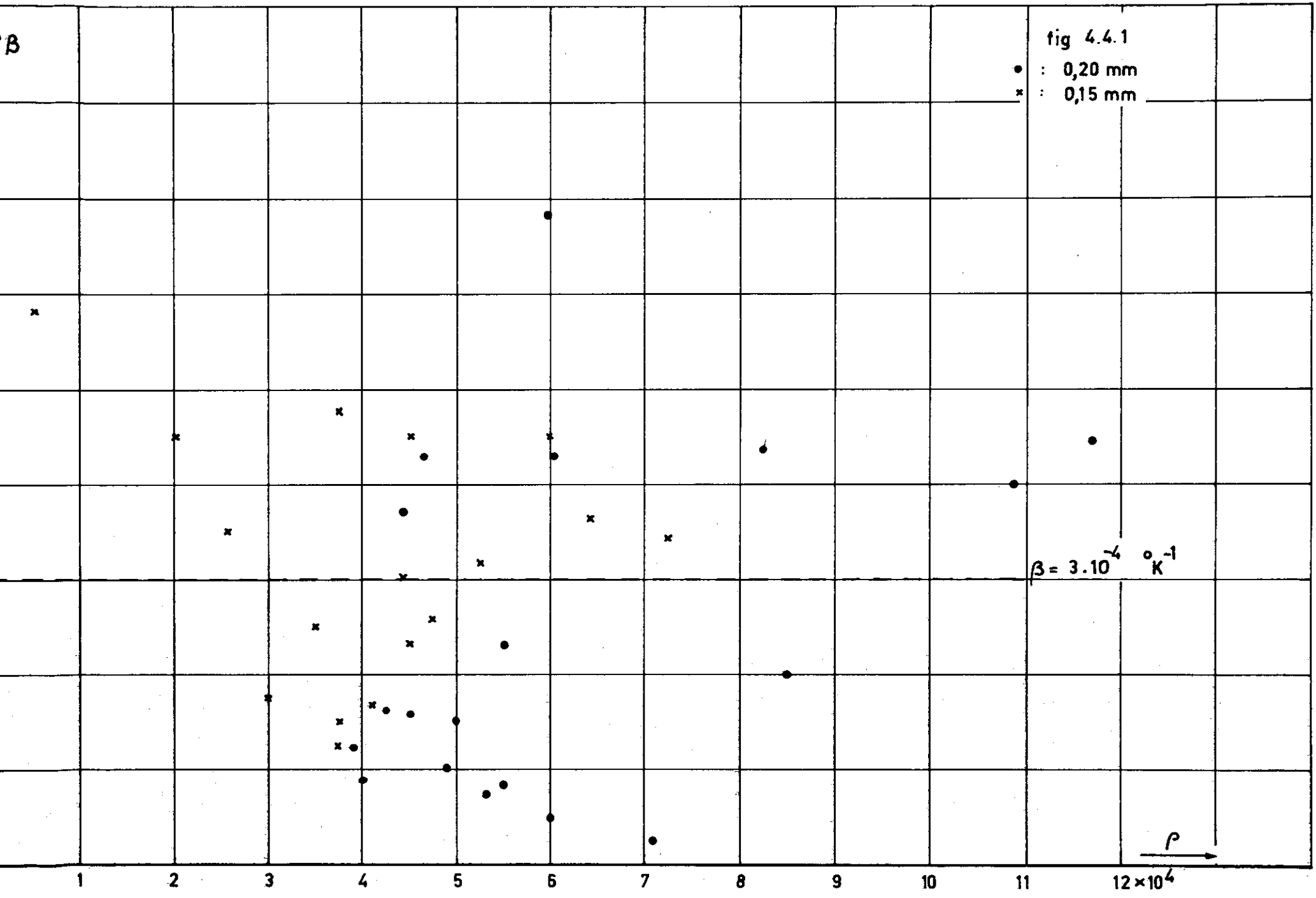
β
fig 4.4.1
• : 0,20 mm
× : 0,15 mm
β = 3.10⁻⁴ °K⁻¹
ρ
1
2
3
4
5
6
7
8
9
10
11
12×10⁴

$10^{-3}\,\Omega$ m and $10^{-4}\,\Omega$ m.

(c) The average value of β according to fig. 2.1b is $6.6.10^{-4}\,{}^{o}K^{-1}$. From fig. 4.4.1 an average value of $\beta = 3.10^{-4}\,{}^{o}K^{-1}$ is found.

(d) The distribution of the values of β as a function of the specific resistance is arbitrary.
An increase in the specific resistance is not connected with an increase in β as is shown in fig. 2.2.1.
Besides to measuring errors, this can be due to the fact that the specific resistance is a function of both temperature and pressure. During the expansion the pressure drop in the discharge may account for a slower rising of the specific resistance (lower values of β) than in the case the pressure is a constant.

The fact that on the whole both the value of ρ and its slope agree with the theoretical values proves that ρ has been calculated with reasonable accuracy. In other words, the values of ρ are correct; accordingly, owing to the relation $\rho = RA$ the cross section A must be computed in the right way. We conclude, therefore, that the diameter of the discharge is the same as the diameter of the channel in which the current flows.

5. Summary and conclusions

This report is the result of an investigation concerning the nature of the physical processes which occur after the evaporation of a fusing silver element, when current interruption does not take place. The conclusions are based upon experimental results as well as upon theoretical calculations.

The process can be described by the sole consideration of the electrical input energy, the internal energy, and the expansion energy.
Other terms are of minor importance.
It was proved that the relation $\alpha_1\sqrt{\Delta p} = \frac{1}{A}\frac{dA}{dt}$ showing the dependency between the average pressure Δp in the discharge and the diameter A of the discharge can be handled successfully. For this kind of experiments the influence of the magnetic pressure is negligible. The experimental values of the specific resistance and its temperature coefficient of a silver discharge, are of the same order of magnitude as the calculated values.

The most important conclusion is that thermal ionisation occurs during and immediately after the evaporation of the wire is completed. The temperature of the gas column if of the order of 10^4.°K. This means that the final stages of the evaporation process occur at a temperature which is much higher than the evaporation temperature of silver at normal pressure (2075°C). At a temperature of 10^4 °K the gas column is about fully ionised, and this indicates a direct transition of electrical conduction, maintained by a liquid metal, to an electrical conduction by an ionised metal vapour.
The mechanism of current interruption, as described by Kriechbaum and Mayr [16, 17] does not apply.

6. Acknowledgements

The work resulting in this report was carried out in the High Voltage - High Current Laboratory of the Technological University Eindhoven, the Netherlands, headed by Prof.Dr. D.Th.J. ter Horst.
The authors thank Mr. G.M.V. van den Bosch, member of this laboratory for his skillful assistance.

Table 1

Most persistent lines of neutral and ionised silver, oxygen and nitrogen. Intensities according to M.I.T. wave-length tables.

	wave-length Å	intensity (arc spectrum)		
Ag I	3281	2000	$5^2P_{3/2} - 5^1S_{\frac{1}{2}}$	resonance lines
	3382	1000	$5^2P_{\frac{1}{2}} - 5^1S_{\frac{1}{2}}$	
	5210	1500	$5^2D_3 - 5^2P_{\frac{1}{2}}$	
	5465	1000	$5^2D_3 - 5^2P_{3/2}$	
Ag II	2246	25		
	2438	60		
N I	4099	150		
	4109	1000		
N II	5666	300		
	5676	100		
	5680	500		

Spark spectrum of the air, most persistent lines

	wave-length	intensity		wave-length	intensity
O	3750	5	N	5679	10
N	3919	6	N	5941	10
N	3995	9	O	7772	10
N	4630				

Table 2

Mach numbers of the different stages of the expansion

d = 0.10 mm

I kA	Mach number first part linear expansion	Mach number second part linear expansion
1.20	14.7	4.0
1.19	14.7	4.0
1.02	25.0	3.8
0.89	18.8	3.7
0.62	14.7	3.3

d = 0.15 mm

2.12	17.0	4.4
1.74	17.9	5.0
1.67	15.1	4.7
1.44	10.0	4.9
1.08	17.0	4.3

d = 0.20 mm

2.99	19.9	6.9
2.52	18.8	4.8
2.48	14.7	4.4
1.97	13.8	4.3
1.71	12.0	3.9

LIST OF REFERENCES

1. L. Vermij — Thesis Techn. University, Eindhoven (1969).

2. L. Spitzer — Physics of fully ionised gases. Intersc. Publ., New York (1962) 23,27.

3. J.H. Park — Nat. Bur. of Stand. RP 1823, 39 (1947).

4. W.M.C. van den Heuvel — Spanningsdelers voor hoge spanningen en gering eigen energieverbruik voor oscillografische metingen. Techn. University, Eindhoven (1963).

5. Handbook of Chemistry and Physics — Chem. Rubber Publ. Co., Cleveland, Ohio (1962)

6. G.C. Chace, H.K. Moore — Exploding Wires, Vol. 1 (1959). Plenum Press, New York.

7. M.L. Lewis, D.B. Sleator — Ball. Res. Lab., Maryland. R.R.L.M. 975 (1956).

8. G.C. Chase, H.K. Moore — Exploding Wires, Vol. 2 (1962). Plenum Press, New York.

9. F.D. Bennett — Phys. Fluids, 5, 8 (1962).

10. E.I. Rester, Shao-Chi Lin, Kantrowitz — J. Appl. Phys. 23, 12 (1952).

11. H.M.J. Pflanz — Steady state and transient properties of electric arcs. Thesis Techn. University, Eindhoven (1967).

12. F.D. Bennett, H.S. Burden, D.D. Shear
Phys. Fluids, 5, 1 (1962).

13. M. Keilhacker Z. f. angew. Phys. 12 (1960) 49.

14. H. Jäger, W. Lochte-Holtgreven
Z. f. Phys. 198 (1967) 351.

15. L. Vermij, P. Boers
De smelttijd en de vervorming van zilverdraden bij verhitting door een elektrische stroom.
Techn. University, Eindhoven (1967).

16. K. Kriechbaum A.E.G. Mitt. 52 (1962) 7/8, 350.

17. O. Mayr E.T.Z. 55 (1934) (31) 757.

18. J. Terpstra Meting der overgangswaarschijnlijkheden bij atomen in het zilverspectrum.
Thesis University of Utrecht (1956).

19. T.J. Tucker J. Appl. Phys. 32, 10 (1961) 1894.

20. I. Holmström, S.K. Händel, B. Stenerhag
J. Appl. Phys. 39, 7 (1968) 2998.